Contract # F49620-92-J-0460

THE OHIO STATE UNIVERSITY

FINAL REPORT ON:

ANALYSIS AND CONTROL OF INTERCONNECTED STRUCTURES

FOR 1992-95

Ü. Özgüner
The Ohio State University
1314 Kinnear Road
Columbus, Ohio 43212

January 1996

Final Report for Period September 1, 1992 - August 31, 1995
RF Project No. 760191/726581

REPORT DOCUMENTATION PAGE	Form Approved OMB No. 0704-0188

1. AGENCY USE ONLY *(Leave blank)*	2. REPORT DATE	3. REPORT TYPE AND DATES COVERED
	JAN 196	Final Technical Report 01 SEP 92 TO 31 AUG 95

4. TITLE AND SUBTITLE
ANALYSIS AND CONTROL OF INTERCONNECTED STRUCTURES

5. FUNDING NUMBERS
F49620-92-J-0460

6. AUTHOR(S)
U. Ozguner

7. PERFORMING ORGANIZATION NAME(S) AND ADDRESS(ES)
The Ohio State University
1314 Kinnear Road
Columbus, OH 43212

8. PERFORMING ORGANIZATION REPORT NUMBER

9. SPONSORING/MONITORING AGENCY NAME(S) AND ADDRESS(ES)
AFOSR/NA
110 Duncan Ave, Suite B 115
Bolling AFB, DC 20332-8050

10. SPONSORING/MONITORING AGENCY REPORT NUMBER
F49620-92-J-0460

11. SUPPLEMENTARY NOTES

12a. DISTRIBUTION AVAILABILITY STATEMENT
Approved for public Release; Distribution Unlimited.

12b. DISTRIBUTION CODE

13. ABSTRACT *(Maximum 200 words)*

The main thrust of our effort has been to consider the control of interconnected rigid and flexible structures. In order to accomplish this, we have utilized different analysis approaches including partial differential equations representing simple substructures and finite element models, radial basis function neural networks and wavelet neural networks representing complex structures. Finally, we have introduced the use of a multiresolutional technique with wavelets. As far as control techniques are concerned, we have concentrated on sliding mode control with a detailed analysis of sampling effects. The controller design in the H2 domain.

14. SUBJECT TERMS	15. NUMBER OF PAGES
	80
	16. PRICE CODE

17. SECURITY CLASSIFICATION OF REPORT	18. SECURITY CLASSIFICATION OF THIS PAGE	19. SECURITY CLASSIFICATION OF ABSTRACT	20. LIMITATION OF ABSTRACT
UNCLASSIFIED	UNCLASSIFIED	UNCLASSIFIED	UL

Standard Form 298 (Rev. 2-89) (EG)
Prescribed by ANSI Std. 239.18
Designed using Perform Pro, WHS/DIOR, Oct 94

ABSTRACT

In this report, we describe the total effort at The Ohio State University on the Project **Analysis and Control of Interconnected Structures**, initiated on September 1, 1992, sponsored by the Air Force Office of Scientific Research (AFSC), under Contract F49620-92-J-0460.

The main thrust of our effort has been to consider the control of interconnected rigid and flexible structures. In order to accomplish this, we have utilized different analysis approaches including partial differential equations representing simple substructures and finite element models, radial basis function neural networks and wavelet neural networks representing complex structures. Finally, we have introduced the use of a multiresolutional technique with wavelets. As far as control techniques are concerned, we have concentrated on sliding mode control with a detailed analysis of sampling effects. The multiresolutional wavelet approach which we concentrated on during the last year has naturally led to a multiresolutional controller design in the H^2 domain.

OVERVIEW

In this report, we describe the total effort at The Ohio State University on the Project **Analysis and Control of Interconnected Structures** which was initiated on September 1, 1992 and sponsored by the Air Force Office of Scientific Research (AFSC) under Contract F49620–92–J–0460.

The first part of this report focuses on sliding mode control for sampled-data systems. In the second part of the report, we concentrate on a generalized sliding mode approach to vibration suppression in flexible structures. Methods for block control of differential-difference systems and a sliding mode approach to control of dispersive flexible structures are discussed. Examples of each method are also presented. The third part of the report emphasizes a general design procedure for radial basis function and wavelet neural networks. Simulation results for these two types of networks based on predicting actuator nonlinearities occurring in a flexible structure. The last part of the report explores uses for time-frequency wavelets. These include the modeling and control of structural systems and subsystems. Versatile structure model based on time-frequency wavelets are developed. A multiresolutional controller which minimizes the sensitivity function for a SISO flexible structure is derived. The controller utilizes the structural models based on time-frequency wavelets. Implementation issues for the multiresolutional controller are also discussed.

Contributors to this three-year research effort were:
Students:
Wu-Chung Su
Layne Lenning
Daniel Clancy
Shyamala Raghunathan

Post-doctoral researchers:
Dr. S. Drakunov

Principal Investigator:
Prof. Ü. Özgüner

A number of publications have appeared based on this project. They are listed in the Appendix.

This project is also linked to AASERT Project F49620-92-J-0299 entitled *Integrated*

Circuits for Distributed Control-(AASERT FY91). The major portion of the research performed by the students supported under this AASERT Project is documented separately. Some of the developments which were produced in the AASERT project are integral to the research reported here and, therefore, are included to produce a stand-alone document.

Contents

List of Figures

List of Tables

1. INTRODUCTION

In this report, we describe the total effort at The Ohio State University on the Project **Analysis and Control of Interconnected Structures**, initiated on September 1, 1992, sponsored by the Air Force Office of Scientific Research (AFSC), under Contract F49620–92–J–0460.

The main thrust of our effort has been to consider the control of interconnected rigid and flexible structures. In order to accomplish this, we have utilized different analysis approaches including partial differential equations representing simple substructures and finite element models, radial basis function neural networks and wavelet neural networks representing complex structures. Finally, we have introduced the use of a multiresolutional technique with wavelets. As far as control techniques are concerned, we have concentrated on sliding mode control with a detailed analysis of sampling effects. The multiresolutional wavelet approach which we concentrated on during the last year has naturally led to a multiresolutional controller design in the H^2 domain.

The following chapters will provide details of the results obtained through the tenure of the project.

In **Chapter 2** several results for sliding mode control of sampled-data systems will be outlined. The sampled-data sliding mode control results will be used to design controllers for a flexible structure. These controllers were verified on an actual flexible structure (which was developed under a previous AFOSR grant).

In **Chapter 3**, we introduce a new approach for vibration damping in flexible structures based on the sliding–mode control approach. Previous use of this approach has been for finite dimensional (approximate) models of flexible structures. Here, we retain the infinite-dimensional model for the structures and investigate exact solutions using sliding–mode control. The use of neural networks in conjunction with this method are also investigated.

In **Chapter 4**, consideration of neural networks let to our development of a new general design procedure for radial basis function neural networks and wavelet neural networks. These type of neural networks are especially well-suited for dealing with irregularly positioned data points. We present simulation results for these two types of networks based on predicting actuator nonlinearities occurring in a flexible structure.

In **Chapter 5**, we explore uses for time-frequency wavelets. These include the modeling and control of structural systems and subsystems. We develop a versatile structure model based on time-frequency wavelets as opposed to the traditional finite element/modal models. The wavelet models are developed for the purpose of being utilized during the controller design phase. We then present some theoretical results

necessary for developing a sensitivity minimization controller based on a wavelet model.

This project is also linked to AASERT Project F49620-92-J-0299 entitled *Integrated Circuits for Distributed Control–(AASERT FY91).* The main results of the research performed by the students supported under this AASERT Project are documented separately, although some of the neural network related efforts are reported here for completeness. (The AASERT document concentrates on related yet distinct efforts of developing and using a FEM analog integrated circuit chip for substructure control.)

2. IMPLEMENTATION OF VARIABLE STRUCTURE CONTROL FOR SAMPLED-DATA SYSTEMS

2.1 Background on Sampled Data Variable Structure Control

The characteristic feature of a continuous time variable structure systems (VSS) is that sliding mode occurs on a prescribed manifold, or switching surface, where switching control is employed to maintain the state on that surface [1, 2, 3, 4, 5]. Since the theory has been originally developed from a continuous time prospective, implementation of sliding mode for sampled-data systems encounters several incompatibilities due to limited sampling rate, sample/hold effect, and discretization errors. As a result, a direct translation of continuous time variable structure control design for discrete implementation leads to the chattering phenomenon in the vicinity of the switching surface.

This chapter deals with the implementation of variable structure control for sampled-data systems by maintaining sliding mode in discrete time. Although a considerable amount of work has been done analyzing discrete time sliding mode, very little was directly addressed to the sampling issues. In [6], Milosavljevic studied the oscillatory characteristic (quasisliding) in the neighborhood of the discontinuity planes due to discretization of continuous time signals. Existence conditions of quasisliding mode were derived as a discrete extension from the continuous time VSS theory. For control law design, Utkin and Drakunov proposed a definition of discrete time equivalent control that directs the states onto the sliding surface in one sampling period [7]. To remain on the surface, the associated control appears to be non-switching. Subsequently, the theoretical basis was furnished with a formal definition of sliding mode for discrete time systems in the context of semigroups [4].

Related works from different prospectives can be found in [8, 9, 10, 11, 12, 13]. Sarpturk *et al.* took a Lyapunov point of view for discrete time linear systems. It was asserted that the switching control be bounded in an open interval to guarantee convergence of sliding motion. This interval was later found to depend linearly on the distance of the state from the switching surface [9], which suggested a nonswitching control when discrete time sliding mode is attained. Sira-Ramirez imposed the geometrical concept to general nonlinear SISO systems along with the existence issues [11]. Parallel results with continuous time VSS's were obtained. To implement discrete time sliding mode control law in compliance with the existence conditions, Furuta proposed the idea of sliding cone (sliding sector), where switching control takes place only when the states are out of the sector, while inside of the sector, the control law remains continuous [10]. Kaynak and Denker used an ARMA model to characterize the control-sliding surface relationship and yielded a non-switching

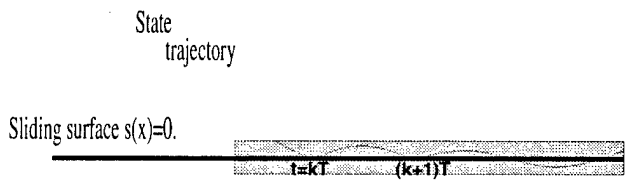

Figure 2.1: Discrete time sliding mode in sampled-data systems

type of control with a predictive-corrective scheme [12]. Bartolini *et al.* incorporated adaptive control strategy to account for system uncertainties and designed control law in terms of a discrete time equivalent control [13].

Our work has mainly extended the original idea of [7] to more general problems with detailed analysis of the sample/hold effects. Preliminary results were reported in [14, 15, 16] and the full development is presented here. The control objective is to maintain the states on the switching surface at each sampling instant. Between samples, the states are allowed to deviate from the surface instead of being constantly and exactly on the switching surface, even the equivalent state travels within a boundary layer of that surface (see Figure 2.1). It will be demonstrated that the thickness of this boundary layer can be reduced significantly by proper consideration of the sampling phenomenon in the control design. Three classes of systems (linear, nonlinear, and stochastic systems) will be investigated individually. Robustness against both internal and external uncertainties will be considered. Furthermore, the chattering problem will be addressed.

The chapter is organized as follows: in Section 2.2, we consider discrete time sliding mode in linear sampled-data systems. The intersample behavior as well as the matching condition will be examined. Robustness against system uncertainties are elaborated. Three types of uncertainties will be studied individually. The overall effects can be treated as a linear combination of the three. In Section 2.3, the results are extended to nonlinear systems. Based on similar assumptions, the control strategies can be directly translated from the linear case. Section 2.4 deals with linear stochastic systems. Sliding mode is defined in terms of a conditional probability function, given the σ-algebra generated by the measured state information. Both cases with continuous measurement and discrete measurement will be considered. To minimize the deviation from the sliding manifold in the mean square sense, the optimal filtering problems will be solved. In each of the above, the chattering phenomenon will be effectively removed with robustness. An experimental example of a flexible structure vibration control is given in section 2.5 to demonstrate the effectiveness of the proposed sampled-data sliding mode control technique. Finally, the conclusion section summarizes the chapter.

2.2 Linear Systems

Consider the dynamic system with a prescribed switching surface

$$\dot{x} = Ax + Bu + Df \tag{2.1}$$
$$\mathcal{S} = \{x | s(x) = Cx = 0\}, \tag{2.2}$$

where the state $x \in R^n$, the control $u \in R^m$, the disturbance vector $f \in R^l$, and the sliding surface vector $s \in R^m$; A, B, D are constant matrices of appropriate dimensions; and the $m \times n$ matrix C is chosen so that the system, when traveling on $\mathcal{S}$, will achieve the desired sliding mode dynamics [2]. We say the disturbance is "rejectable" if there exists a control u that can eliminate its effect instantaneously in the dynamic system. If the closed loop system behavior does not depend on $f(t)$, we say the controlled system is disturbance invariant. It is well known that the matching condition [3]

$$rank[B, D] = rank[B] \tag{2.3}$$

has to be satisfied for the system ((2.1)) to be disturbance invariant in sliding mode.

The discrete time representation of the dynamic equation ((2.1)) is obtained by applying u through a zero-order-hold:

$$x_{k+1} = \Phi x_k + \Gamma u_k + d_k, \tag{2.4}$$

where $\Phi = e^{AT}$, $\Gamma = \int_0^T e^{A\lambda} d\lambda B$, $d_k = \int_0^T e^{A\lambda} Df((k+1)T - \lambda) d\lambda$. Note that the magnitude of Γ and d_k are both $O(T)$ if $f(t)$ is bounded.

The discrete time sliding mode control is to steer the states towards and maintain them on the surface $\mathcal{S}$ at each sampling instant such that

$$s_k = Cx_k = 0 \quad k \geq k_s. \tag{2.5}$$

During the sampling interval $kT \leq t < (k+1)T$, the state will deviate from $\mathcal{S}$. The following Lemma provides bounds on the deviation from the sliding surface.

Lemma 1 If the disturbance $f(t)$ in ((2.1)) is bounded and smooth in the intersample interval $kT \leq t \leq (k+1)T$, then $\begin{cases} s_k = 0 \\ s_{k+1} = 0 \end{cases}$ implies $s(t) = O(T^2)$ during that sampling period.

The $O(T^2)$ deviation is inevitable for sampled-data systems. It is the ultimate performance a sampled controller can attain for continuous time plants. Note that if $s_k = (T^2)$ and $s_{k+1} = O(T^2)$, the intersample value of the sliding surface vector is still $O(T^2)$.

The sample/hold effect not only destroys perfect sliding mode as depicted above, it also invalidates the complete disturbance rejection property for the discrete time system ((2.4)).

Lemma 2 The sampled-data system ((2.4)) is disturbance invariant on the discrete time sliding manifold ((2.5)) only if the continuous time matching condition ((2.3)) holds.

The above lemma states the necessity of the continuous time matching condition, however, the sufficiency is not confirmed. The zero-order-hold is applied to the control variables only. A similar "hold" does not take place in the disturbance channels. In general, the discrete time disturbance d_k will not lie in the range space of the control coefficient matrix Γ and hence can not be rejected completely even if discrete time sliding mode occurs.

Although perfect sliding mode and complete disturbance rejection are not possible in sample-data systems, one can still maintain the states in the vicinity of the sliding surface and retain satisfying disturbance rejection character by proper consideration of the sampling phenomenon in the control design.

We will consider three different types of uncertainties that are important in affecting a dynamic system's behavior; namely, exogenous disturbances, system parameter variations, and control coefficient variations. It will be shown that these uncertainties can be rejected to at least $O(T^2)$ accuracy and that the chattering phenomenon inhabiting in continuous time variable structure systems can be removed.

Since the control in the sampled data system will show jumps from the continuous time point of view, the formal concept of continuity is not compatible with the notion of discrete time control. In order to make the analogy in between, let us introduce the following definition:

Definition 1 The discrete time control law u_k is said to be equivalent to discontinuous if $\Delta u_k = O(1)$, continuous if $\Delta u_k = O(T)$, smooth if $\Delta^2 u_k = O(T^2)$, where Δ denotes the backward differencing operator $1 - z^{-1}$.

To avoid a cumbersome description, the "continuity" of discrete time control to appear in the following text will refer to its equivalent meaning as defined above.

2.2.1 Exogenous Disturbances

Consider the case when only the exogenous disturbance $f(t)$ is present. We define the discrete time equivalent control by solving $s_{k+1} = 0$ [7], which leads to

$$u_k^{eq} = -(C\Gamma)^{-1}C(\Phi x_k + d_k) \tag{2.6}$$

assuming $C\Gamma$ is invertible. Note that u_k^{eq} is generally not accessible because it requires the value of d_k, which depends on the future values of the disturbance $f(t)$ from the present sampling instant kT to the next one $(k+1)T$. It is impossible to evaluate d_k exactly unless $f(t)$ is known. Nevertheless, with boundedness and smoothness assumptions imposed on $f(t)$, d_k can be predicted by its previous value d_{k-1} [17], which can be computed from ((2.4)). The error is

$$d_k - d_{k-1} = \int_0^T e^{A\lambda} D \int_{kT-\lambda}^{(k+1)T-\lambda} \dot{f}(\sigma) d\sigma d\lambda = O(T^2)$$

assuming $\dot{f}(t)$ is bounded. To approximate u_k^{eq}, we define

$$u_k^{in} = -(C\Gamma)^{-1}C(\Phi x_k + d_{k-1}). \tag{2.7}$$

Taking the Taylor's series expansion of Φ yields the relationship $C\Phi x_k = s_k + (AT + \frac{T^2}{2!}A^2 \cdots)x_k$. Since the magnitude of $C\Gamma$ and Cd_{k-1} are both $O(T)$, in order that u_k^{in} be admissible, the magnitude of $C\Phi x_k$ must also be $O(T)$. In other words, x_k must lie within an $O(T)$ boundary layer of $\mathcal{S}$ (or $s_k = O(T)$) for u_k^{in} to be admissible.

In order to define the boundary layer of the sliding surface, let us adopt the following notation:

$\mathcal{S}_T = \{x_k | u_k^{in} \in \mathcal{U}\}$ is the $O(T)$ boundary layer of $\mathcal{S}$.

We propose the variable structure control law

$$u_k = \begin{cases} -(C\Gamma)^{-1}C(\Phi x_k + d_{k-1}) & \text{when } x_k \in \mathcal{S}_T, \\ -(C\Gamma)^{-1}C(\Phi x_k + d_{k-1} - s_k + Ksgn(s_k)), & \\ & \text{otherwise.} \end{cases} \tag{2.8}$$

The positive definite matrix K will determine the stepsize for the state to approach the boundary layer $\mathcal{S}_T$. The magnitude of K has to be chosen small enough not to overshoot $\mathcal{S}_T$.

Theorem 1 For a linear sampled-data system ((2.4)) with the exogenous disturbance satisfying the matching condition ((2.3)), the effect of $f(t)$ can be reduced to $O(T^2)$ if the variable structure control law ((2.8)) is applied.

2.2.2 System Parameter Variations

Consider a dynamic system subject to parameter variations

$$\dot{x} = (A + \Delta A(t))x + Bu. \tag{2.9}$$

The matching condition for the uncertainty $\Delta A(t)$ is

$$Rank[\Delta A(t)\Theta,\ B] = Rank[B] \quad \forall t, \tag{2.10}$$

where Θ is an $n \times (n-m)$ matrix with the columns forming a basis of the subspace $null(C)$ [3]. The unknown $\Delta A(t)x$ may be treated as a disturbance. The associated sampled-data representation is given in ((2.4)), where

$$d_k = \int_0^T e^{A\lambda} \Delta A((k+1)T - \lambda)x((k+1)T - \lambda)d\lambda. \tag{2.11}$$

Assuming $\Delta\dot{A}(t)$ is bounded, d_k can be predicted by d_{k-1} with $O(T^2)$ error, and we have the following theorem.

Theorem 2 For a linear system with parameter variations ((2.9)), the control ((2.8)) will lead to $s_{k+1} = O(T^2)$ if $\Delta A(t)$ satisfies the matching condition ((2.10)). Furthermore, the state will attenuate to zero asymptotically.

2.2.3 Control Coefficient Matrix Variations

Systems with unknown control coefficient matrix variations have the following dynamic equation

$$\dot{x} = Ax + (B + \Delta B(t))u. \tag{2.12}$$

The matching condition is

$$Rank[\Delta B(t),\ B] = Rank[B] \quad \forall t. \tag{2.13}$$

The system dynamic equation in discrete time is the same as ((2.4)), where

$$d_k = \Delta\Gamma_k u_k,$$
$$\Delta\Gamma_k = \int_0^T e^{A\lambda}\Delta B((k+1)T - \lambda)d\lambda.$$

Employing the control law u_k^{in} induces a dynamic feedback in u_k through d_{k-1}. Since

$$s_{k+1} = C\Phi x_k + C(\Gamma + \Delta\Gamma_k)u_k, \tag{2.14}$$

the stability of s_k implies stability in x_k, which ensures stability in u_k if $C(\Gamma + \Delta\Gamma_k)$ is invertible.

Introduce the following notation:

$$e_{\Delta\Gamma_k} = \Delta\Gamma_k - \Delta\Gamma_{k-1}, \quad \Delta_k = C\Delta\Gamma_k(C\Gamma)^{-1}. \tag{2.15}$$

The quantity Δ_k can be regarded as a measure of variations in the control coefficient matrix with respect to the known one Γ. If $\Delta B(t)$ and $\Delta\dot{B}(t)$ are bounded, we have $e_{\Delta\Gamma_k} = O(T^2)$ and $\Delta_k = O(1)$.

Lemma 3 For the linear system with control coefficient matrix variation ((2.12)), if $\Delta B(t)$ satisfies the matching condition ((2.13)); and the states x_{k-1}, x_k are in the boundary layer $\mathcal{S}_T$, then the control u_k^{in} will lead to

$$s_{k+1} = -2\Delta_k s_k + \Delta_{k-1}s_{k-1} + \delta_k \tag{2.16}$$

with $\delta_k = O(T^2)$.

Stability of s_k in ((2.16)) can be assured if Δ_k is small enough; that is, the variation of $\Delta B(t)$ is small with respect to B. Since the quantity δ_k is $O(T^2)$, the state will enter the $O(T^2)$ boundary layer of $\mathcal{S}$ if ((2.16)) is stable.

Theorem 3 The state x_k attenuates to zero asymptotically if

1. *The conditions in Lemma 3 hold.*
2. *Equation ((2.16)) is stable.*
3. *The $m \times m$ matrix $C(\Gamma + \Delta\Gamma_k)$ is nonsingular.*

If all three types of uncertainties are present in the dynamic equation, the variable structure control law ((2.8)) can still be employed to compensate the uncertainties simultaneously. In this case, d_k is the lumped effect of all disturbances, the resultant

sliding mode accuracy is $s(t) = O(T^2)$. As long as the states remain in the $O(T^2)$ boundary layer of the sliding surface, u_k^{in} becomes continuous and chattering in the control is removed.

Theorem 4 The control u_k^{in} is continuous if $s_{k-1} = O(T^2)$. Furthermore, u_k approaches the continuous time equivalent control as the sampling rate approaches infinity.

$$u_k \xrightarrow{T \to 0} u^{eq}(t) = -(CB)^{-1}C(Ax + Df). \tag{2.17}$$

2.3 Nonlinear Systems

In the previous sections, we have developed a discrete time sliding mode control method applied to linear sampled-data systems to alleviate chattering. Here, we extend it to nonlinear systems. We assume the nonlinearities and uncertainties are bounded and smooth, in this case the past values of the states can be utilized to predict the effect. This approach allows us to keep the state in the $O(T^2)$ vicinity of the sliding manifold.

Consider the nonlinear system

$$\dot{x} = a(x) + b(x)u + v(x,t) \tag{2.18}$$

with a prescribed sliding manifold

$$\mathcal{S} = \{x | s(x) = 0\}, \tag{2.19}$$

where $a(x)$ and $b(x)$ are known differentiable functions with dimensions $n \times 1$ and $n \times m$ respectively; $v(x,t)$ is an $n \times 1$ unknown vector-valued differentiable function. The disturbance matching condition is

$$Rank[b(x), v(x,t)] = Rank[b(x)] \text{ when } x \in \mathcal{S}. \tag{2.20}$$

Let $G(x) = \frac{\partial}{\partial x}s(x)$ be the $m \times n$ Jacobian matrix of $s(x)$ so that the dynamics of the sliding surface vector can be expressed as

$$\dot{s}(x) = G(x)a(x) + G(x)b(x)u + G(x)v(x,t). \tag{2.21}$$

Applying a zero-order-hold to the control yields the discrete time representation of ((2.18)) and ((2.21))

$$
\begin{aligned}
x_{k+1} = \; & x_k + \int_{kT}^{(k+1)T} a(x)dt + \int_{kT}^{(k+1)T} b(x)dt\, u_k \\
& + \int_{kT}^{(k+1)T} v(x,t)dt
\end{aligned} \tag{2.22}
$$

$$
\begin{aligned}
s_{k+1} = \; & s_k + \int_{kT}^{(k+1)T} G(x)a(x)dt + \int_{kT}^{(k+1)T} G(x)b(x)dt\, u_k \\
& + \int_{kT}^{(k+1)T} G(x)v(x,t)dt.
\end{aligned} \tag{2.23}
$$

The control objective is to keep the states x_k on the sliding surface $\mathcal{S}$ in discrete time

$$
s(x_k) = 0, \quad \text{for} \quad k \geq k_s \tag{2.24}
$$

The following Lemma is the nonlinear version of Lemma 2.

Lemma 4 The sampled-data system ((2.22)) is disturbance invariant on the discrete time sliding manifold ((2.24)) only if the continuous time matching condition ((2.20)) holds.

2.3.1 Matched Disturbances

Consider the system ((2.18)), in which the disturbance $v(x,t)$ satisfies the matching condition ((2.20)). Introduce the notation:

$$
\begin{aligned}
F_k &= \int_{kT}^{(k+1)T} G(x)a(x)dt \\
B_k &= \int_{kT}^{(k+1)T} G(x)b(x)dt \\
h_k &= \int_{kT}^{(k+1)T} G(x)v(x,t)dt
\end{aligned} \tag{2.25}
$$

so that the discrete representation ((2.23)) can be rewritten as

$$
s_{k+1} = s_k + F_k + B_k\, u_k + h_k. \tag{2.26}
$$

The equivalent control is

$$
u_k^{eq} = -B_k^{-1}(s_k + F_k + h_k) \tag{2.27}
$$

assuming B_k is invertible. The magnitude of F_k, B_k, and h_k is $O(T)$ if $G(x)$, $a(x)$, $b(x)$, and $v(x,t)$ are bounded. F_k, B_k, and h_k usually cannot be evaluated exactly since they depend on the future value of the state and the unknown disturbance. Nevertheless, with some mild smoothness condition on the functions $G(x), a(x), b(x)$ and $v(x,t)$, they can be approximated by the following expressions:

$$\begin{aligned}\bar{F}_k &= G(x_k)a(x_k)T \\ \bar{B}_k &= G(x_k)b(x_k)T \\ \bar{h}_k &= s_{k+1} - s_k - \bar{F}_k - \bar{B}_k.\end{aligned} \tag{2.28}$$

With ((2.28)), we obtain an approximation for the equivalent control ((2.27))

$$u_k^{in} = -\bar{B}_k^{-1}(s_k + \bar{F}_k + \bar{h}_{k-1}), \tag{2.29}$$

where $\bar{B}_k$ is invertible by assumption. Similar to ((2.7)), x_k must lie in the boundary layer $\mathcal{S}_T$ for u_k^{in} to be admissible. The proposed variable structure control law is:

$$u_k = \begin{cases} -\bar{B}_k^{-1}(s_k + \bar{F}_k + \bar{h}_{k-1}) & \text{when } x_k^{in} \in \mathcal{S}_T \\ -\bar{B}_k^{-1}(Ksgn(s_k) + \bar{F}_k + \bar{h}_{k-1}) & \text{otherwise} \end{cases} \tag{2.30}$$

Theorem 5 If the disturbance in dynamic system ((2.18)) satisfies the matching condition ((2.20)), then the effect of $v(x,t)$ can be reduced to $O(T^2)$ if the control ((2.30)) is applied.

2.3.2 Control Coefficient Variations

Consider the case when there is an unknown variation $\tilde{b}(x)$ in the control coefficient

$$\dot{x} = a(x) + b(x)u + \tilde{b}(x)u. \tag{2.31}$$

The matching condition is

$$Rank[b(x),\ \tilde{b}(x)] = Rank[b(x)] \quad \text{when} \quad x \in \mathcal{S}. \tag{2.32}$$

Following the same discretization procedure yields the discrete representation indicated in ((2.26)) with

$$\begin{aligned} h_k &= \tilde{B}_k u_k \\ \tilde{B}_k &= \textstyle\int_{kT}^{(k+1)T} G(x)\tilde{b}(x)dt. \end{aligned}$$

Introduce the following notation:

$$\begin{aligned} &e_{\bar{F}_k} = F_k - \bar{F}_k, && \bar{e}_{\bar{F}_k} = \bar{F}_k - \bar{F}_{k-1}, && \epsilon_{F_k} = F_k - F_{k-1}, \\ &e_{\bar{B}_k} = B_k - \bar{B}_k, && \bar{e}_{\bar{B}_k} = \bar{B}_k - \bar{B}_{k-1}, && \\ &e_{B_k} = B_k - B_{k-1}, && e_{\tilde{B}_k} = \tilde{B}_k - \tilde{B}_{k-1}, && \\ &e_{h_k} = h_k - h_{k-1}, && e_{\bar{h}_k} = h_k - \bar{h}_k && \\ &\Delta_k = \tilde{B}_k B_k^{-1}, && \epsilon_{\Delta_k} = \Delta_k - \Delta_{k-1}. && \end{aligned} \tag{2.33}$$

It can be proved that $\Delta_k = O(1)$, $\epsilon_{\Delta_k} = O(T)$, and $e_{j_k} = O(T^2)$, $\bar{e}_{j_k} = O(T^2)$, where $j = F,\ B,\ \bar{F},\ \bar{B},\ \hat{B}$.

Lemma 5 When the state is in the boundary layer $\mathcal{S}_T$, the following equalities are true:

$$s_{k+1} = h_k - h_{k-1} + \alpha_k^1(2s_k - s_{k-1}) + \alpha_k^2 \tag{2.34}$$
$$h_k = -\Delta_k[(s_k + F_k + h_{k-1}) + \beta_k^1(2s_k - s_{k-1}) + \beta_k^2], \tag{2.35}$$

where $\alpha_k^1 = O(T)$, $\alpha_k^2 = O(T^2)$, $\beta_k^1 = O(T)$, $\beta_k^2 = O(T^2)$.

The equalities in Lemma (5) can be obtained by direct substitution from ((2.33)) and ((2.29)) into ((2.26)). Furthermore,

$$\begin{aligned}
\alpha_k^1 &= -2e_{\bar{B}_k}\bar{B}_k^{-1} \\
\alpha_k^2 &= -e_{\bar{B}_k}B_k^{-1}F_k + e_{\bar{F}_k} + e_{\bar{B}_k}\bar{B}_k^{-1}e_{\bar{F}_k} + e_{\bar{h}_{k-1}} \\
&\quad + e_{\bar{B}_k}\bar{B}_k^{-1}(\bar{F}_{k-1} + \bar{B}_{k-1}u_{k-1}) \\
\beta_k^1 &= e_{\bar{B}_k}B_k^{-1} \\
\beta_k^2 &= -e_{\bar{F}_k} - e_{\bar{h}_{k-1}}e_{\bar{B}_k}\bar{B}_k^{-1}(e_{\bar{F}_k} - \bar{B}_{k-1}u_{k-1}).
\end{aligned} \tag{2.36}$$

They serve as preparation for the theorem stated below:

Theorem 6 For the nonlinear system with control coefficient matrix variation ((2.31)), the control ((2.30)) will lead to $s_k \to O(T^2)$ asymptotically if

1. The state lie in the boundary layer $\mathcal{S}_T$.
2. The variation $\tilde{b}(x)$ satisfies the matching condition ((2.32)) and that $\dot{\tilde{b}}(x)$ is bounded.
3. The following dynamic equation for s_k is stable.

$$s_{k+1} = a_k^0 s_k + a_k^1 s_{k-1} + a_k^2 s_{k-2} + \delta_k, \tag{2.37}$$

where

$$
\begin{aligned}
a_k^0 &= -2\Delta_k - 2\Delta_k\beta_k^1 + 2\alpha_k^1 = -2\Delta_k + O(T) \\
a_k^1 &= \Delta_{k-1} + 2\Delta_k\alpha_k^1 - \epsilon_{\Delta_k} + \Delta_k\beta_k^1 + 2\Delta_{k-1}\beta_k^1 - \alpha_k^1 \\
&= \Delta_{k-1} + O(T) \\
a_k^2 &= \epsilon_{\Delta_k} - \Delta_k\alpha_k^1 - \Delta_{k-1}\beta_k^1 = O(T) \\
\delta_k &= -\Delta_k e_{F_k} - \epsilon_{\Delta_k} F_{k-1} + \Delta_k\alpha_k^2 \\
&\quad +\epsilon_{\Delta_k}(F_{k-2} + B_{k-2}u_{k-2}) \\
&\quad -\Delta_k\beta_k^2 + \Delta_{k-1}\beta_{k-1}^2 + \alpha_k^2 = O(T^2).
\end{aligned}
$$

If the sampling rate is sufficiently high, the dynamic equation ((2.37)) is reduced to second order

$$s_{k+1} = -2\Delta_k s_k + \Delta_{k-1}s_{k-1}. \tag{2.38}$$

This agrees with ((2.16)), the result for linear systems. Stability of s_k can be assured if Δ_k is small enough; that is, the variation of the control coefficient $\check{g}(x)$ is small with respect to $b(x)$. If the $O(T)$ terms in ((2.37)) are not negligible, the dynamic equation for s_k becomes third order with an $O(T^2)$ input. Stability of ((2.37)) implies that $s_k \to O(T^2)$ asymptotically.

2.4 Stochastic Systems

This section is devoted to discrete time sliding mode control for continuous time linear systems with stochastic disturbances. The disturbance is assumed to satisfy an Ito type stochastic differential equation [18]

$$dx = Axdt + Budt + (D\xi dt + Rdw_1) \tag{2.39}$$

$$d\xi = W\xi dt + Qdw_2, \tag{2.40}$$

where $w_1(t)$, $w_2(t)$ are independent standard Wiener processes. Here $D\xi$ represents the colored part of the noise and the formal expression $R\frac{dw_1}{dt}$, the white part. Without loss of generality, the autocovariance matrices of the white noises are assumed to be identity.

We consider two possible state information channels: continuous measurement and discrete measurement. To compensate for the stochastic disturbances with a sampling controller, a mixed continuous-discrete type of filtering problem will be solved if continuous state information $x(t)$ is used. On the other hand, the use of discrete state information x_k will lead to a discrete time optimal filtering problem. In both cases, we apply the following assumption:

Assumption 1

1. *W has asymptotically stable eigenvalues;*

2. *R is full rank;*

3. *The processes $Rw_1(t)$ and $Qw_2(t)$ are uncorrelated.*

2.4.1 Continuous Measurement

Consider the discrete time version of ((2.39))

$$x_{k+1} = \Phi x_k + \Gamma u_k + \eta_k + v_k, \tag{2.41}$$

where $\eta_k = \int_{kT}^{(k+1)T} e^{A((k+1)T-\lambda)} D\xi(\lambda)d\lambda$ is the colored part of the disturbance and $v_k = \int_{kT}^{(k+1)T} e^{A((k+1)T-\lambda)} R dw_1(\lambda)$ is a white noise. Since the white noise can not be compensated, the control objective is to minimize the effect of the colored part η_k in the sampled-data system ((2.41)). Applying the control law with an estimation of η_k

$$u_k = -(C\Gamma)^{-1} C\Phi x_k - (C\Gamma)^{-1} C\hat{\eta}_k, \tag{2.42}$$

we obtain

$$s_{k+1} = C(\eta_k + v_k - \hat{\eta}_k). \tag{2.43}$$

For u_k ((2.42)) to be admissible, it still requires that the state lie in the $O(T)$ boundary layer $\mathcal{S}_T$. This boundary layer can be defined similarly as in the previous sections. Here, we only consider when $x_k \in \mathcal{S}_T$.

In the presence of stochastic disturbances, sliding mode is defined in terms of a probability measure. To minimize $E\|s_{k+1}\|^2$ given the observation of $x(t)$ up to the instant kT, the estimate $\hat{\eta}_k$ should be picked as a conditional expectation

$$\hat{\eta}_k = E(\eta_k | \mathcal{F}_{kT}), \tag{2.44}$$

where $\mathcal{F}_t$ denotes a σ-algebra generated by the process $x(t)$

$$\mathcal{F}_t = \sigma\{x(\tau) | 0 \le \tau \le t\}. \tag{2.45}$$

Since $w_1(t)$ is a martingale [18], the estimation η_k is obtained by taking a conditional expectation given the σ-algebra $\mathcal{F}_{kT}$

$$\hat{\eta}_k = \int_{kT}^{(k+1)T} e^{A((k+1)T-\lambda)} D d\lambda \hat{\xi}(kT) = \Xi \hat{\xi}_k, \tag{2.46}$$

where the matrix Ξ is of the form

$$\Xi = \int_0^T e^{W\lambda} D d\lambda, \tag{2.47}$$

and $\hat{\xi}$ is a conditional expectation

$$\hat{\xi}(t) = E(\xi(t)|\mathcal{F}_t). \tag{2.48}$$

Therefore, from ((2.46)) it suggests that in order to obtain the values of $\hat{\eta}_k$ we need a filter to calculate $\hat{\xi}_k$. The following theorem provides the form of such a filter.

Theorem 7 If assumption (1) holds, the optimal estimate of ξ_k is

$$\hat{\xi}_k = z_k + LR^T x_k, \tag{2.49}$$

where z_k satisfies

$$z_k = \Lambda z_{k-1} + \zeta_{k-1} + \Pi u_{k-1} \tag{2.50}$$

with Λ, Π and ζ_k defined by:

$$\begin{array}{l} \Lambda = e^{HT}, \\ \Pi = \int_0^T e^{H\lambda} d\lambda M, \\ \zeta_{k-1} = \int_{(k-1)T}^{kT} e^{H(kT-\lambda)} N x(\lambda) d\lambda, \end{array} \tag{2.51}$$

where the matrices H, N, M, L are

$$\begin{array}{l} H = W - LR^T D, \\ N = -LR^T A + WLR^T - LR^T DLR^T, \\ M = -LR^T B, \\ L = PD^T R(R^T R)^{-2} \end{array} \tag{2.52}$$

and P is the positive definite solution of the algebraic matrix Ricatti equation

$$PW^T + WP - PD^T R(R^T R)^{-2} R^T DP + QQ^T = 0. \tag{2.53}$$

The filter ((2.49)) and ((2.50)) provides a way to calculate the conditional expection of ξ_k given the information from the continuous time process $x(t)$. Substituting the estimate into the equation ((2.46)) we obtain an optimal $\hat{\eta}_k$ as:

$$\hat{\eta}_k = \Xi(z_k + LR^T x_k). \tag{2.54}$$

The quantity $\eta_k + v_k - \hat{\eta}_k$ from the right hand side of ((2.43)) is a discrete-time white noise process with variance of order $O(T)$. It means that the mean square deviation of s_{k+1} from zero is of order $O(T^{\frac{1}{2}})$.

2.4.2 Discrete Measurement

Suppose we only have access to the discrete state information, the σ-algebra generated by the discrete measurement x_k, x_{k-1}, $\cdots$ is

$$\mathcal{F}_k = \sigma\{x_j | 0 \leq j \leq k\}. \tag{2.55}$$

The discrete time representations of ((2.39)) and (??) to be considered are

$$x_{k+1} = \Phi x_k + \Upsilon \xi_k + \Gamma u_k + v_k + \nu_k \tag{2.56}$$

$$\xi_{k+1} = \Psi \xi_k + q_k, \tag{2.57}$$

where $\nu_k = \int_0^T e^{A(T-\lambda)} D \int_0^\lambda e^{W(\lambda-\tau)} Q dw_2(kT+\tau) d\lambda$, $q_k = \int_{kT}^{(k+1)T} e^{W((k+1)T-\lambda)} Q dw_2(\lambda)$ are discrete white noises generated form the process dw_2; the matrices Ψ and Υ are

$$\Psi = e^{WT}, \qquad \Upsilon = e^{AT} \int_0^T e^{-A\lambda} D e^{W\lambda} d\lambda. \tag{2.58}$$

To minimize the effect caused by ξ_k, we apply the control law

$$u_k = -(C\Gamma)^{-1} C\Phi x_k - (C\Gamma)^{-1} C\Upsilon \hat{\xi}_k, \tag{2.59}$$

where $\hat{\xi}_k$ is the optimal estimation of ξ_k given $\mathcal{F}_k$

$$\hat{\xi}_k = E(\xi_k | \mathcal{F}_k). \tag{2.60}$$

From ((2.56)), the discrete measurements x_k and x_{k-1} yield the innovation process

$$y_{k-1} = x_k - \Phi x_{k-1} - \Gamma u_{k-1} = \Upsilon \xi_{k-1} + v_{k-1} + \nu_{k-1}. \tag{2.61}$$

Combining ((2.61)) with ((2.57)), one can construct a stationary Kalman filter with the process noise q_{k-1} in ((2.57)) correlated with the measurement noise $(v_{k-1} + \nu_{k-1})$ in ((2.61)) through dw_2. To obtain a standard Kalman filter formulation with uncorrelated noises, we rewrite equation ((2.40))

$$\xi_{k+1} = \bar{\Psi}\xi_k + \bar{H}\bar{R}^{-1}y_k + \bar{q}_k, \tag{2.62}$$

where $\bar{H}$ and $\bar{R}$ are the covariance matrices

$$\bar{H} = E(q_k(v_k + \nu_k)^*), \quad \bar{R} = E((v_k + \nu_k)(v_k + \nu_k)^*),$$

and $\bar{\Psi}$, $\bar{q}_k$ are defined as

$$\bar{\Psi} = \Psi - \bar{H}\bar{R}^{-1}\Upsilon, \quad \bar{q}_k = q_k - \bar{H}\bar{R}^{-1}(v_k + \nu_k).$$

With ((2.62)) and the innovation process y_k, an optimal estimation for ξ_k is acquired

$$\hat{\xi}_k = \bar{\Psi}\hat{\xi}_{k-1} + \bar{H}\bar{R}^{-1}y_{k-1} + \bar{L}(y_{k-1} - \Upsilon\hat{\xi}_{k-1}), \tag{2.63}$$

$$\bar{L} = \bar{P}\Upsilon^T(\Upsilon\bar{P}\Upsilon^T + \bar{R})^{-1}, \tag{2.64}$$

$$\bar{P} = \bar{\Psi}(\bar{P} - \bar{P}\Upsilon^T(\Upsilon\bar{P}\Upsilon^T + \bar{R})^{-1}\Upsilon\bar{P})\bar{\Psi}^T + \bar{Q}\bar{Q}^T, \tag{2.65}$$

where $\bar{Q}^T$ is the autocovariance matrix of the discrete white noise $\bar{q}_k$ in ((2.62)).

Applying the control law ((2.59)) yields

$$s_{k+1} = C(\Upsilon\xi_k + v_k + \nu_k - \Upsilon\hat{\xi}_k). \tag{2.66}$$

The quantity $\Upsilon(\xi_k - \hat{\xi}_k) + v_k + \nu_k$ from the right hand side of ((2.66)) is also a discrete time white noise with variance of order $O(T)$. Therefore, the mean square deviation of s_{k+1} from the sliding surface is $O(T^{\frac{1}{2}})$.

2.5 Experimental Example – $O(T^2)$ Sliding Mode Control on a Flexible Structure

This section deals with sampled-data implementation of sliding mode for a flexible structure control problem. We apply the sampled-data sliding mode control techniques to a flexible structure developed for Large Interconnected Vibration Experiment (LIVE) at the Ohio State University. The truss structure, constructed of hollow PVC tubes and Noryl nodes, is aligned on a vertically cantilevered configuration shown in Figure 2.2.

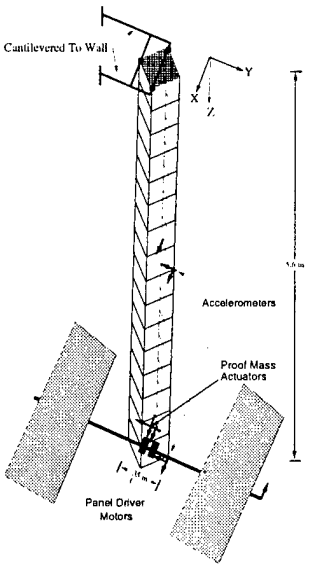

Figure 2.2: LIVE truss structure

The physical properties, control hardware setups, preliminary dynamic modelling and experimental results were published in [19] by Redmill and Özgüner. Extended works in sampled-data sliding mode control experiment are presented here.

The dynamic equations of the vertically cantilevered truss can be modelled based on the Euler-Bernoulli beam formulation. The bending motion is discribed by a fourth order partical differential equation (PDE).

$$\rho A\ddot{Q} + EIQ'''' = 0 \tag{2.67}$$

where EI is the bending stiffness of the truss, A is the cross-sectional area and ρ is the density. The independent variable along the length of the truss is z, t is time, and $Q(z,t)$ is the flexural displacement.

The boundary conditions (BC) with one fixed end and one with an end mass M_L are given as

$$\begin{aligned} &Q(0,t) = 0 \\ &Q'(0,t) = 0 \\ &-EIQ''(l,t) = 0 \\ &EIQ'''(l,t) - M_L\ddot{Q}(l,t) = -u(t) \end{aligned} \tag{2.68}$$

To solve for $Q(z,t)$, one can follow the standard Fourier method and convert the PDE into infinite assumed modes which are driven parallelly by the boundary control $u(t)$.

Each mode can be expressed as a second order underdamped oscillation equation.

$$Q(z,t) = \sum_{i=1}^{\infty} q_i(t)\phi_i(z) \tag{2.69}$$

$$\ddot{q}_i + 2\xi_i w_i \dot{q}_i + w_i^2 q_i = k_i u(t), \quad i = 1, 2, \cdots \tag{2.70}$$

where $\phi_i(z)$ is the spatially dependent mode shape coefficient, $q_i(t)$ is the time dependent modal state, w_i is the modal frequency, ξ_i is the damping ratio, and k_i is control gain for each mode. The system parameters are given in [19] and [20].

Control action is obtained using proof-mass actuators with neglected actuator dynamics. Sensing of truss motion is accomplished through a piezoelectric accelerometer mounted on the structure to measure the relative velocity between the proof-mass actuator and the structure.

Combining the dynamic equation ((2.70)) with the actuation and sensing mechanism, we come up with the following I/O relationship:

$$y(t) = y_0(t) + \sum_{i=1}^{\infty} y_i(t) \tag{2.71}$$

$$\ddot{y}_i(t) + 2\xi_i w_i \dot{y}_i(t) + w_i^2 y_i(t) = k_i \dot{u}(t), i = 1, 2, \cdots, \tag{2.72}$$

where $y(t)$ is the velocity measurement obtained from the output of the accelerometer; $y_0(t)$ is a low frequency (~ 0.1 Hz) measurement noise; $y_i(t), i = 1, 2, \cdots$ is the flexural velocity for each mode.

With the system parameters w_i, ξ_i, k_i, we obtain a state space representation for each mode of interest

$$\begin{aligned} \dot{x}_i &= A_i x_i + B_i u, \\ y_i &= C_i x_i, \end{aligned} \tag{2.73}$$

where $x_i = [q_i \ \dot{q}_i]^T$ is an 2×1 modal state vector, u is th e scaler control, y_i is the bending velocity of mode i,

$$A_i = \begin{bmatrix} 0 & 1 \\ -w_i^2 & -2\xi_i w_i \end{bmatrix}, \ B_i = \begin{bmatrix} 0 \\ b_i \end{bmatrix}, C_i = [0 \ c_i] \tag{2.74}$$

and

$$b_i c_i = k_i. \tag{2.75}$$

There are infinitely many possible choices for b_i and c_i satisfying ((2.75)). For simplicity, we choose

$$b_i = \sqrt{|k_i|}, \quad c_i = sgn(k_i)\sqrt{|k_i|} \tag{2.76}$$

The sampling frequency throughout this experiment is 100 Hz, which corresponds to sampling period $T = 0.01$ second. The experimental results presented here are for the first flextural mode only. To demonstrate the effectiveness of the proposed control method, we take the following senario:

Part 1: $0 \leq t < 2$ Settlement - $u_k = 0$.

Part 2: $2 \leq t < 12$ Shake up the truss - $u_k = 0.3 \sin(w_1 \cdot kT)$.

Part 3: $12 \leq t < 20$ Sliding mode control v.s. No control.

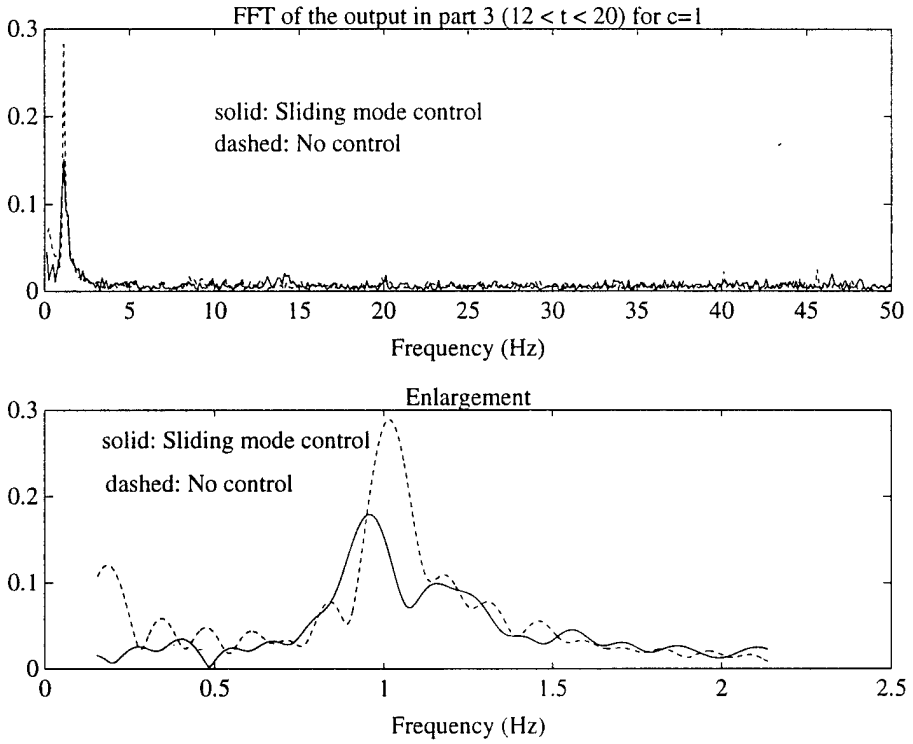

Figure 2.3: Frequency content: Sliding mode control (c=1) v.s. No control

The sliding surface for the second order vibrating system is chosen as

$$s(x) = [c \;\; 1]x_1 = cq_i + \dot{q}_1 = 0.$$

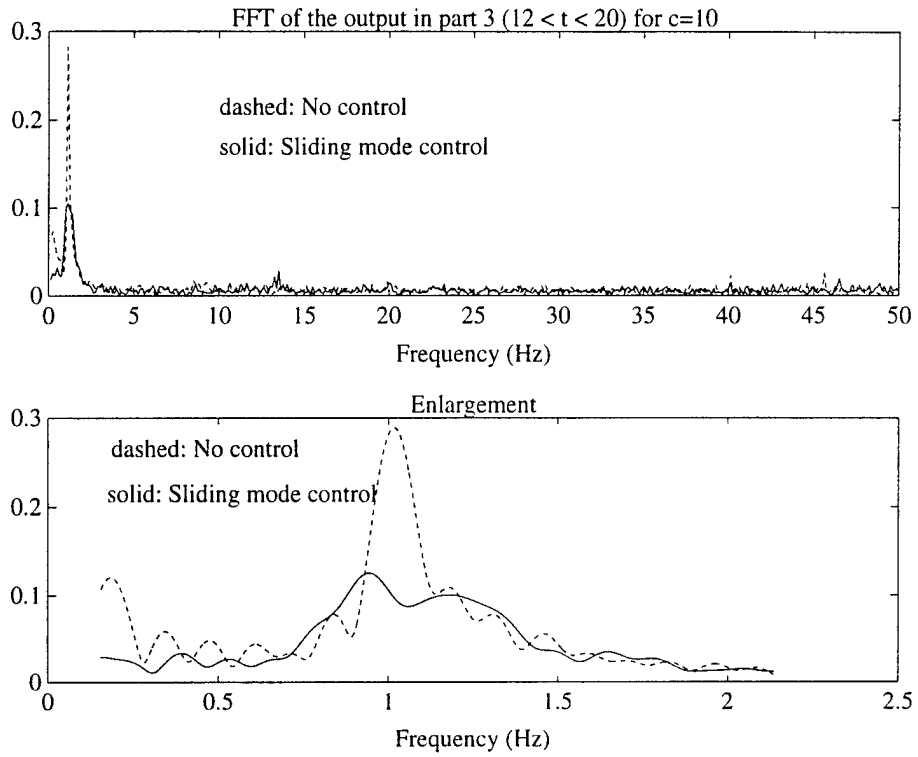

Figure 2.4: Frequency content: Sliding mode control (c=10) v.s. No control

Experiments are conducted for $c = 1$ and $c = 10$. A saturation function is employed to limit the applied control

$$u_k = Sat(u_k^{eq}, 0.1).$$

Figure 2.3 depicts the frequency content (FFT) of y_k in Part 3 for $c = 1$. Similar result for $c = 10$ is shown in Figure 2.4, in which better performance is obtained.

3. VIBRATION SUPPRESSION IN FLEXIBLE STRUCTURES VIA GENERALIZED SLIDING MODES

In this chapter the problem of supressing vibrations in flexible sructures by means of sliding-mode control is considered. Sliding mode control algorithms for flexible structures have been used previously, but these were based on finite-dimensional models (see for example [22] and [23]).

Sliding mode control provides stable and robust closed loop systems for finite-dimensional plants, but the direct application of this design technique based on approximate models of flexible structures, may lead to undesirable performance of the infinite-dimensional system. This phenomenon is due to the delays which are inherent in such systems. The presence of delays can be explained by wave propagation across the structure. If the control is applied to the boundary of the flexible structure, its action can influence other parts of the structure only after the wave caused by the actuation propagates and reaches those parts. In the case of large flexible structures, these delays are not small and cannot be neglected. The application of sliding mode control ignoring these effects leads to chattering and may not be successful.

Here we consider mathematical models in the form of partial differential equations (PDE) that permit us to take into account the features described above. Therefore, more appropriate control algorithms may be designed.

The generalization of the sliding mode control concept to systems with delays and for more general dynamic systems described by semigroups of state space transformations was originally considered in [4], [24]. We base our approach on this concept, which can be called *manifold control.* The design procedure is divided into two steps. In the first step, the manifold is designed in such a way that it will be an integral manifold for the closed loop system. In the second step, the control which forces the system to move along this manifold must be found. The crucial point of the problem is to design the integral manifold which guarantees system stabilization.

In this chapter, the nondispersive wave equation is chosen as a canonical form for distributed parameter systems described by partial differential equations. Since the nondispersive wave equation is equivalent to a system with delay, this allows for the transformed system to use sliding mode control algorithms developed earlier for systems of differential-difference equations [4].

Subsequently, a class of flexible structures with fourth order spatial partial derivatives is considered by using the same technique. This is accomplished by going through a two stage process where they are initially transformed into the second order form analyzed originally.

The problem of designing the control law which assigns the desired stable integral manifold to the system can be solved by using any of several different methods (including linear methods). The use of sliding modes, however, makes the closed loop system highly insensitive to external disturbances and parameter variations.

3.1 Generalization of the Sliding Mode Control Concept

There are two aspects in traditional sliding mode control design: the choice of the sliding surface and control synthesis in the reduced order space. From the point of view of dynamic system theory, the sliding surface is just a stable integral manifold of the closed loop system, with a specific property that in the area of attraction the system state is absorbed by the manifold in finite time.

For finite dimensional systems in $\mathbb{R}^n$ modeled as

$$\dot{x} = f(x), \tag{3.1}$$

such manifolds can exist only if the right hand side does not satisfy the well known Lipschitz condition

$$|f(x) - f(y)| < L|x - y|, \tag{3.2}$$

which is usually used to guarantee the uniqueness of the solution both for $t \geq t_0$ and $t < t_0$.

Let $F(t; t_0, x_0)$ be a solution of the system of ordinary differential equations (3.1) with initial condition $x(t_0) = x_0$, i.e. a transition function. Then the Lipschitz condition implies that F is defined for $t \geq t_0$ and $t < t_0$. The family of state space transformations $F(t; t_0, .)$ is a group with respect to the composition operation. The inverse element to $F(t; t_0, .)$ is $F(t_0; t, .)$. For an asymptotically stable integral manifold, the trajectory initiated in its vicinity tends to, but never reaches it.

In contrast to systems of equations whose right-hand sides satisfy the Lipschitz condition, in systems with discontinuities there are integral manifolds which can be reached in finite time.

Consider the system in $\mathbb{R}^n$

$$\dot{x} = f(x) + B(x)u, \tag{3.3}$$

where $f(x)$, $B(x)$ are functions which satisfy the Lipschitz condition, and $u \in \mathbb{R}^m$ is discontinuous on the smooth surfaces $\{x : s_i(x) = 0\}$ $i = 1, 2, \ldots, m$ in $\mathbb{R}^n$:

$$u_i(x) = \begin{cases} u_i^+(x) & \text{if } s_i(x) > 0 \\ u_i^-(x) & \text{if } s_i(x) < 0 \end{cases} \tag{3.4}$$

If the sliding mode exists on the intersection of discontinuity surfaces $\sigma = \bigcap_{i=1}^{m} \{x : s_i(x) = 0\}$ then

1. σ is an integral manifold since it consists of the system trajectories;
2. the uniqueness of the inverse to the shift operator $F(t; t_0, .)$ does not hold on σ since each piont on σ can reached from at least two different points: from outside (because of the finite time of convergence) and from points on the manifold. This is a characteristic feature of sliding mode and it is taken as a basis for the generalization of the sliding mode concept.

The general definition of a dynamic system in any metric space $\mathcal{X}$ (including those under consideration described by partial differential equations) utilizes a description in the form of a transition operator F similar to the one considered above. The following Definition was introduced in [4]

Definition 1 $x \in \mathcal{X}$ is said to be a sliding point at the time instant t if an equation $F(t; t_0, \xi) = 0$ for every $t_0 < t$ has more than one solution ξ.

This Definition implies that the sliding manifolds are asymptotically stable manifolds to which the system state converges in finite time from any initial condition in the area of attraction.

The underlying philosophy of the proposed approach as applied to PDE models of flexible structures is the same as in any sliding mode control design for finite dimensional systems. After representing the system in a "convenient" form, a sliding manifold is chosen and then the control is designed such that the system state reaches this manifold in finite time and then "slides" along it. The control in this case is not necessarily discontinuous.

3.2 Block Control of Differential-Difference Systems

In this section we shall consider a class of composite systems in block form [25] and [26] comprized of blocks of differential equations coupled with blocks of difference equations. We shall demonstrate that sliding mode controllers may be effectively utilized in driving the state to zero.

We consider two configurations:
Configuration A

$$\dot{x}(t) = A_{11}x(t) + A_{12}z(t) \tag{3.5}$$
$$z(t) = A_{21}x(t-\tau) + A_{22}z(t-\tau) + B_0u(t-\tau), \tag{3.6}$$

Configuration B

$$z(t) = A_{11}z(t-\tau) + A_{12}x(t-\tau) \tag{3.7}$$
$$\dot{x}(t) = A_{21}z(t) + A_{22}x(t) + B_0u(t). \tag{3.8}$$

It is assumed that $x \in \mathbb{R}^{n_1}$, $z \in \mathbb{R}^{n_2}$ and $u \in \mathbb{R}^m$. A_{11}, A_{12}, A_{21}, A_{22}, B_0 are matrices of appropriate dimensions. Since A_{12} is not necessarily a full rank matrix, we can use the representation:

$$A_{12} = B_1C_2, \tag{3.9}$$

where B_1 and C_2 have full column and row rank respectively. We assume that the pairs (A_{11}, B_1) in both types of configurations are controllable and the system (C_2, A_{22}, B_0) is invertible.

Denoting $v = C_2z$ we consider it as a new control variable in (3.5), (3.7) and as the output variable for (3.6) and (3.8).

In the first block of **Configuration A**

$$\dot{x}(t) = A_{11}x(t) + B_1v(t) \tag{3.10}$$

we use sliding mode control $v(x) = col(v_1, \ldots, v_{n2})$ to provide stability

$$v_i(x) = \begin{cases} v_i^+(x) & \text{if } s_i(x) > 0 \\ v_i^-(x) & \text{if } s_i(x) < 0. \end{cases} \tag{3.11}$$

The sliding manifold for this block is

$$\sigma_0 = \{x : s(x) = 0\}, \tag{3.12}$$

where $s = col(s_1, \ldots, s_{n2})$.

Since the second block (3.6) is the difference system, under the invertibility condition it is possible to find a control u which provides the desired discontinuous function for the output $v(x) = C_2z$ [4]. This equality defines another manifold in the system state space

$$\sigma_1 = \{(x, z) : v(x) - C_2 z = 0\}. \tag{3.13}$$

As a result, the state slides on the intersection $\sigma = \sigma_0 \cap \sigma_1$. That means we can assign any desired rate of stability for the closed loop system (3.5)-(3.6).

For the system in **Configuration B** the design procedure is different. On the first step we find a linear control $v = Dz(t)$ for the first block (3.7)

$$z(t) = A_{11} z(t - \tau) + B_1 v(t - \tau) \tag{3.14}$$

to establish stability for the difference system (3.7), which can be achieved by using the sliding mode control on some manifold σ_2 system as described in the previous section. Then the problem is to steer $s = Dz(t) - C_2 x(t)$ to zero or to reach the manifold

$$\sigma_3 = \{(x, z) : s(x, z) = 0\}. \tag{3.15}$$

We solve this problem in the class of sliding-mode control algorithms:

$$u_i(x) = \begin{cases} u_i^+(x) & \text{if } s_i(x) > 0 \\ u_i^-(x) & \text{if } s_i(x) < 0. \end{cases} \tag{3.16}$$

The resulting motion again will occur on the intersection $\sigma = \sigma_2 \cap \sigma_3$.

3.3 Sliding-Mode Control for Suppressing Vibrations of a Flexible Bar

As a first example we consider the longitudinal or torsional oscillations of a flexible bar. The control is assumed to be a force or torque applied at one end of the bar, the other end is free. Let Q be the displacement of the bar from the unexcited position. We then have the following equations for a unit bar with normalized parameters [27]:

$$\frac{\partial^2 Q(t, x)}{\partial t^2} = \frac{\partial^2 Q(t, x)}{\partial x^2} \tag{3.17}$$

$$\frac{\partial Q(t, 0)}{\partial x} = -u(t) \tag{3.18}$$

$$\frac{\partial Q(t, 1)}{\partial x} = 0, \tag{3.19}$$

where x is the position along the rod and $u(t)$ denotes the actuation force or torque. Applying the Laplace transform to equation (3.17) and boundary conditions (3.18), (3.19) under zero initial conditions

$$Q(0,x) = 0, \tag{3.20}$$

$$\frac{\partial}{\partial x}Q(0,x) = 0, \tag{3.21}$$

we will have:

$$p^2\hat{Q}(p,x) = \hat{Q}''(p,x) \tag{3.22}$$

$$\hat{Q}'(p,0) = -\hat{u}(p) \tag{3.23}$$

$$\hat{Q}'(p,1) = 0, \tag{3.24}$$

where $\hat{Q}(p,x) = \mathcal{L}Q(t,x)$, $\hat{u}(p) = \mathcal{L}u(t)$.

The solution of this boundary value problem for the ordinary differential equation (3.22) is

$$\hat{Q}(p,x) = \frac{e^{p(x-1)} + e^{-p(x-1)}}{e^p - e^{-p}}\frac{1}{p}\hat{u}(p). \tag{3.25}$$

The solution of the stabilization problem depends greatly on what point of the bar is considered as the system output. We shall consider the free end of the bar as an output (thus this is the noncollocated actuator/sensor case).

$$y(t) = Q(t,1). \tag{3.26}$$

From (3.25) we obtain

$$\hat{y}(p) = \hat{Q}(p,1) = \frac{2}{e^p - e^{-p}}\frac{1}{p}\hat{u}(p). \tag{3.27}$$

In the time domain the correspondence between $u(t)$ and $y(t)$ may be written as

$$\dot{y}(t+1) - \dot{y}(t-1) = 2u(t) \tag{3.28}$$

or

$$\dot{y}(t) - \dot{y}(t-2) = 2u(t-1). \tag{3.29}$$

We can now write this equation in the form of the differential-difference system **Configuration A** by introducing a new variable z:

$$\dot{y}(t) = z(t) \tag{3.30}$$
$$z(t) = z(t-2) + 2u(t-1). \tag{3.31}$$

The block representation of the differential-difference system simplifies the developement of the control algorithm. Considering the variable $z(t)$ in the first block (3.30) as the control, we can obtain sliding-mode [1] by assigning

$$z(t) = -\lambda sgn(y(t)). \tag{3.32}$$

This equality is valid if

$$s(t) = z(t) + \lambda sgn(y(t)) = 0. \tag{3.33}$$

To achieve the above, we can use the control

$$u(t) = -\frac{1}{2}z(t-1) - \frac{1}{2}\lambda sgn(y(t+1)). \tag{3.34}$$

This control algorithm seems to be noncausal, however using an extrapolator it can in fact be realized as an operator on the current and the past values of the control variables. To demonstrate this, solve equation (3.30) taking $y(t)$ as an initial condition:

$$y(t+1) = y(t) + \int_t^{t+1} z(\tau)d\tau. \tag{3.35}$$

or using (3.31)

$$y(t+1) = y(t) + \int_{t-1}^{t} (z(\tau-1) + 2u(\tau))d\tau = y(t) + y(t-1) - y(t-2) + 2\int_{t-1}^{t} u(\tau)d\tau \tag{3.36}$$

since $\dot{y}(t) = z(t)$. Substituting $y(t+1)$ from this expression to (3.34) and again using the fact that $z(t) = \dot{y}(t)$ we will have:

$$u(t) = -\frac{1}{2}\dot{y}(t-1) - \frac{1}{2}\lambda sgn(y(t) + y(t-1) - y(t-2) + 2\int_{t-1}^{t} u(\tau)d\tau). \tag{3.37}$$

With this control the system (3.30),(3.31) and therefore (3.17) is stabilized in finite time.

3.4 Dispersive Flexible Structures: an Integral Transformation Approach

The problem of supressing vibrations in the systems described by second order partial differential equations as studied in the previous sections was reduced to those for a differential-difference system. The delay in these systems is due to the nondispersive properties of such structures. The Euler-Bernoulli beam is an example of a dispersive structure. In this section we consider the Euler-Bernoulli beam and other dispersive structures of the second and fourth order.

Consider now the problem of supressing normal vibrations along a unit length flexible beam described by equations of fourth order. One end of the beam is assumed to be clamped while a control force is applied to the other. The Euler-Bernoulli model of the beam with normalized parameters is :

$$\frac{\partial^2 Q(t,x)}{\partial t^2} = -\frac{\partial^4 Q(t,x)}{\partial x^4} \tag{3.38}$$

$$Q(t,0) = 0 \tag{3.39}$$

$$Q'(t,0) = 0 \tag{3.40}$$

$$Q''(t,1) = 0 \tag{3.41}$$

$$Q'''(t,1) = u(t). \tag{3.42}$$

where $'$ denotes partial differentiation with respect to the spatial variable x.

The main idea of our approach is to reduce the order of the controlled part of the system by applying an integral transformation:

$$P(t,\xi) = \int_0^1 \mathcal{D}(\xi,x)Q(t,x)dx. \tag{3.43}$$

Here $P(t,\xi)$ is a new controlled variable and ξ is a new independent spatial variable $(0 \leq \xi < \infty)$. The kernel of the transformation $\mathcal{D}$ is assumed to satisfy the same type of boundary value problem as Q but with homogeneous boundary conditions.

$$\frac{\partial^2 \mathcal{D}(\xi, x)}{\partial \xi^2} = -\frac{\partial^4 \mathcal{D}(\xi, x)}{\partial x^4}. \tag{3.44}$$

$$\mathcal{D}(\xi, 0) = 0 \tag{3.45}$$

$$\mathcal{D}'(\xi, 0) = 0 \tag{3.46}$$

$$\mathcal{D}''(\xi, 1) = 0 \tag{3.47}$$

$$\mathcal{D}'''(\xi, 1) = 0. \tag{3.48}$$

ξ in this equation is analogous to a time variable and its values can change from zero to infinity.

It has been shown [28] that under these conditions $P(t, \xi)$ satisfies an equation of the second order with control in the right hand side:

$$\frac{\partial^2 P(t, \xi)}{\partial t^2} = \frac{\partial^2 P(t, \xi)}{\partial \xi^2} + \varphi(\xi) u(t), \tag{3.49}$$

where

$$\varphi(\xi) = -\mathcal{D}(\xi, 1). \tag{3.50}$$

In this equation in contrast to that with $\mathcal{D}$, ξ is a spatial variable.

We can say that the transformation (3.43) "absorbs" the dispersive properties of the flexible structure as equation (3.49) describes how the waves are travelling there without changing their form. For more details on this approach and a more general formulation, see [28].

3.5 Use of Neural Networks with the Integral Transformation Approach

For a given point, $\xi = \xi^*$, the integral transformation

$$P(t, \xi^*) = \int_0^1 D(\xi^*, x) Q(t, x) dx \tag{3.51}$$

may be realized with the aid of an artificial neural network as shown in Figure 3.1. As shown previously, $P(t, \xi^*)$ can be realized as the output of a differential-difference

system of the form of (3.5)–(3.6) with input $u(t)$. Rather than solving for $D(\xi^*, x)$ and performing the integral transformation analytically, a neural network may be trained to perform these tasks. It should be noted that the transformation is a functional depending only on x and ξ^*–not on t.

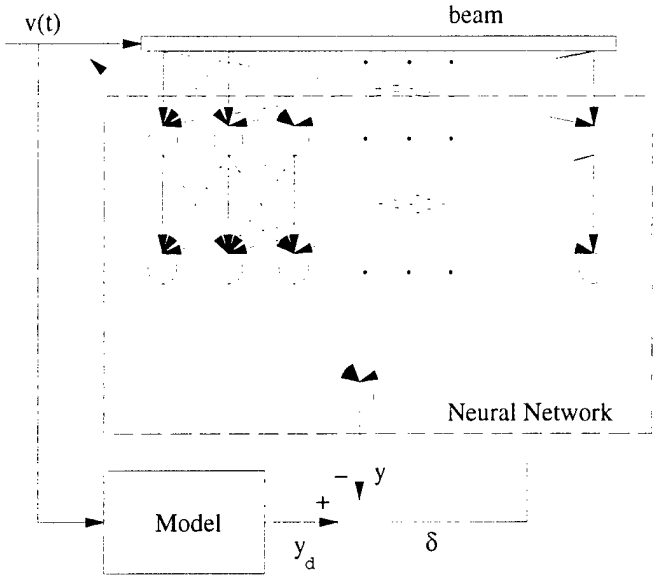

Figure 3.1: Configuration for Training Neural Network

The input $u(t)$ is assumed to excite both the beam and the differential-difference model (3.5)–(3.6). The output of the neural network $y^t = O^t$ is compared to $y_d^t = P(t, \xi^*)$ which is the output of the differential-difference model. The error $\delta^t = y_d^t - y^t$ is then used to train the neural network using some training algorithm such as the standard backpropagation techniques.[29, 30]

The activation function of each neuron may arbitrarily chosen to be any differentiable function $\mathcal{F}(h)$. At some time t, the activation of the i^{th} neuron in any of the layers is given by

$$a_i^t = \mathcal{F}(h_i^t) \tag{3.52}$$

where h_i^t is the total input for the i^{th} neuron

$$h_i = \sum_j w_{ij} \tilde{a}_j^t + \theta_i \tag{3.53}$$

where $\tilde{a}_j^t$ is the output of the j^{th} neuron in the preceding layer.

Using the standard quadratic error measure for time t,

$$E^t = \frac{1}{2}\left[y_d^t - y^t\right]^2, \tag{3.54}$$

and the overall measure of error $E = \sum_t E^t$, the neural network is trained using a gradient descent algorithm to adjust the weights. Variations to the standard back-propagation algorithm such as inclusion of a momentum term in the update rule have been found to be useful in speeding the convergence of the network

$$\Delta w_{ij}(t+1) = -\eta \frac{\partial E}{\partial w_{ij}} + \alpha \Delta w_{ij}(t) \tag{3.55}$$

where $w_{ij}(t+1) = w_{ij}(t) + \Delta w_{ij}(t)$.

For proper training of the neural network, all modes of interest of the beam must be excited. Therefore, the input to the beam, $u(t)$, or any initial conditions must be sufficiently rich to excite these modes of interest. Also, due to the computational intensity of training an artificial neural network, it is advantageous to train the network off-line.

Once the neural network has been trained, the network becomes the first stage of the controller as shown in Figure 3.2. The output of the neural network is fed to the sliding-mode controller which has been designed for the differential-difference model.

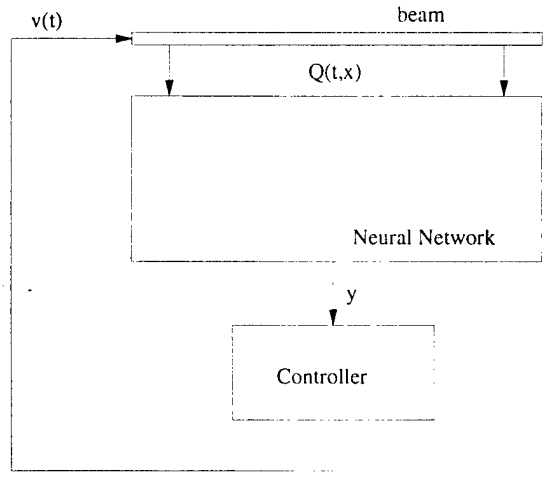

Figure 3.2: Closed Loop System with Neural Network

Simulations of an Euler-Bernoulli beam example and more details of this work may be found in [31].

4. RADIAL BASIS FUNCTION NEURAL NETWORKS AND WAVELET NEURAL NETWORKS

The application of artificial neural networks for solving learning problems and for approximating nonlinear functions has occurred in various fields at a frenzied pace. A good summary/introduction into the field of neural networks can be found in [29]. When solving general pragmatic learning problems, the training data tends to be irregularly distributed over the input space. The radial basis function methodology is an approach for multivariable interpolation which is especially well-suited for dealing with irregularly positioned data points. The radial basis function technique constructs a function space which is linear and depends on a distance measure between the known data points. The idea of a multiresolution learning network or wavelet network is to have the capability of dealing with irregularly positioned data points, generalizing the nonlinear relationship between the given inputs and desired outputs, and being able to capture the desired fine details of the nonlinear mapping. This chapter presents a general procedure for designing neural networks. The procedure is applicable to both radial basis function neural networks and wavelet neural networks.

4.1 Radial Basis Function Networks

A radial basis function (RBF) neural network (RBFNN) is a network composed of input vectors $\mathbf{X}_i = [\ x_{i1}\ \ x_{i2}\ \ \cdots\ \ x_{ip}\ ]^T$, $\mathbf{X}_i \in I\!R^p$ and output vectors $\mathbf{Y}_i = [\ y_{i1}\ \ y_{i2}\ \ \cdots\ \ y_{iq}\ ]$, $\mathbf{Y}_i \in I\!R^q$ for $i = 1,2,\ldots,r$ exemplars with a hidden layer of radially symmetric kernel activation functions. According to Broomhead and Lowe [32], the RBFNN is given by the mapping $y_{ik} : I\!R^p \rightarrow I\!R,\ \ \forall i = 1,2,\ldots,r$

$$y_{ik} = \lambda_{0k} + \sum_{j=1}^{L} \lambda_{jk}\, \phi\left(\frac{\|\mathbf{X}_i - \mathbf{C}_j\|}{\sigma_j}\right) \qquad \forall k = 1,2,\ldots,q \tag{4.1}$$

where: $\mathbf{Y}_i = [\ y_{i1}\ \ y_{i2}\ \ \cdots\ \ y_{iq}\ ]$

y_{ik} is kth output element for ith exemplar

λ_{0k} represents the output bias for the kth element of the output vector

L is the number of kernel neurons

λ_{jk} is the weight between jth kernel node and kth output element

$\phi(\mathbf{z}) : I\!R^+ \rightarrow I\!R \triangleq$ Radial Basis Function

$\mathbf{C}_j \in I\!R^p$ represents the centroid vector for the jth kernel RBF

The solution to (4.1) yields a set of linear equations for the NN weights λ_{jk} which can be given as follows:

$$\left[\begin{array}{ccc} \boldsymbol{\Upsilon}_1 & \cdots & \boldsymbol{\Upsilon}_q \end{array} \right] = \boldsymbol{\Theta} \left[\begin{array}{ccc} \boldsymbol{\Lambda}_1 & \cdots & \boldsymbol{\Lambda}_q \end{array} \right] \tag{4.2}$$

Making the following definitions:

$$\left[\begin{array}{ccc} \boldsymbol{\Upsilon}_1 & \cdots & \boldsymbol{\Upsilon}_q \end{array} \right] \triangleq \left[\begin{array}{ccc} y_{11} & \cdots & y_{1q} \\ \vdots & \ddots & \vdots \\ y_{m1} & \cdots & y_{mq} \end{array} \right] \tag{4.3}$$

$$\left[\begin{array}{ccc} \boldsymbol{\Lambda}_1 & \cdots & \boldsymbol{\Lambda}_q \end{array} \right] \triangleq \left[\begin{array}{ccc} \lambda_{01} & \cdots & \lambda_{0q} \\ \lambda_{11} & \cdots & \lambda_{1q} \\ \vdots & \ddots & \vdots \\ \lambda_{M1} & \cdots & \lambda_{Mq} \end{array} \right] \tag{4.4}$$

$$\boldsymbol{\Theta} \triangleq \left[\begin{array}{cccc} 1 & \phi(\|\mathbf{X}_1 - \mathbf{C}_1\|) & \cdots & \phi(\|\mathbf{X}_1 - \mathbf{C}_M\|) \\ 1 & \phi(\|\mathbf{X}_2 - \mathbf{C}_1\|) & \cdots & \phi(\|\mathbf{X}_2 - \mathbf{C}_M\|) \\ \vdots & \vdots & \ddots & \vdots \\ 1 & \phi(\|\mathbf{X}_m - \mathbf{C}_1\|) & \cdots & \phi(\|\mathbf{X}_m - \mathbf{C}_M\|) \end{array} \right] \tag{4.5}$$

and closely examining (4.2) shows that the vectors of network weights $\boldsymbol{\Lambda}_k$ can be solved for independently by considering only the $\boldsymbol{\Upsilon}_k$ output. Since the system of equations (4.2) are decoupled, the RBF network can be uniquely determined by considering it as q multiple input, single output (MISO) systems. The NN output weights, λ_{jk}, can be found by solving the corresponding linear least squares optimization problem.

When developing a RBFNN, the primary design parameters to be determined consist of choosing appropriate centroids, $\mathbf{C}_j$, and smoothing factor(s), σ_j. RBFNN performance is critically dependent upon the selected centroids and smoothing factors. Several methods are commonly used for selecting appropriate centroids. One approach uses the standard k-means clustering algorithm [33], [34], as an iterative process over the entire set of training data. The other approach uses the standard k-means clustering algorithm as an adaptive process in real time [34]. The common method for determining the smoothing factor(s) is the heuristic known as "P nearest-neighbor" [35]. The primary problem encountered with these selection procedures is that the resultant RBF networks tend to have a large number of kernel nodes, and some even have poor performance. Chen, Cowan and Grant [36] have developed a systematic

approach to selecting the most significant centers from a set, usually large, of candidate centers. The approach by Chen, *et al.* [36] uses an orthogonal least squares (OLS) procedure in a forward regression manner to determine the significant centers to within a specified tolerance ρ, $0 < \rho < 1$. The selection of the tolerance ρ is the key to balancing the accuracy and complexity of the final RBF neural network design.

4.2 Wavelet Neural Network Architecture 1

One wavelet network structure follows readily from a reconstruction formula for any function in Hilbert space, $f \in \mathcal{H}$, based on the discrete wavelet transform coefficients for the function given by Daubechies [37]

$$f = \frac{2}{A+B} \sum_{m,n \in \mathbb{Z}} \langle f, \psi_{m,n} \rangle \, \psi_{m,n} \quad for \;\; (B/A - 1) \ll 1 \tag{4.6}$$

as long as there exist $A > 0$ and $B < \infty$ satisfying

$$A\|f\|^2 \leq \sum_{m,n \in \mathbb{Z}} | \langle f, \psi_{m,n} \rangle |^2 \leq B\|f\|^2 \tag{4.7}$$

where: $\langle x, y \rangle$ represents the inner product
$\langle f, \psi_{m,n} \rangle$ represents the discrete wavelet transform coefficients
$\{\psi_{m,n}(x) = {a_0}^{-m/2} \psi({a_0}^{-m} x - n b_0) \;\; \forall m, n \in \mathbb{Z}\}$ represents a discrete family of wavelets
A and B represent the frame bounds

When the frame bounds satisfy the condition, $A = B$, the frame becomes a tight frame, and if $\|\psi_{m,n}\| = 1 \; \forall m, n \in \mathbb{Z}$, then the $\psi_{m,n}$ constitute an orthonormal basis for $\mathcal{H}$, Daubechies [37]. In general, frames, whether tight or not, are not orthonormal bases, but instead simply span $\mathcal{H}$, i.e. admit redundancy in representing any $f \in \mathcal{H}$. Thus, the wavelet network given by equation (4.8) can approximate any function in $\mathcal{H}$, or for more practical purposes $\mathcal{L}^2(\mathbb{R})$.

One form of the feedforward wavelet neural network (WNN) architecture is a network composed of input vectors $\mathbf{X}_i = [\; x_{i1} \;\; x_{i2} \;\; \cdots \;\; x_{ip} \;]^T$, $\mathbf{X}_i \in \mathbb{R}^p$ and output vectors $\mathbf{Y}_i = [\; y_{i1} \;\; y_{i2} \;\; \cdots \;\; y_{iq} \;]$, $\mathbf{Y}_i \in \mathbb{R}^q$ for $i = 1, 2, \ldots, r$ exemplars with a hidden layer of wavelet activation functions. According to [38],[39], the feedforward WNN can be represented by the mapping $y_{ik} : \mathbb{R}^p \rightarrow \mathbb{R}, \quad \forall i = 1, 2, \ldots, r$

$$y_{ik} = \lambda_{0k} + \sum_{j=1}^{L} \lambda_{jk} \, \psi(diag(\mathbf{a}_j)\mathbf{X}_i - \mathbf{b}_j) \quad \forall k = 1, 2, \ldots, q \tag{4.8}$$

where: $\psi(\mathbf{z}) \triangleq$ Mother Wavelet Function
$\text{diag}(\mathbf{a}_j)$ represents a diagonal matrix whose elements are $\mathbf{a}_j$
$\mathbf{a}_j = diag(a0^{-m_{j,1}}, \ldots, a0^{-m_{j,p}}) \in I\!R^p$ is the dilation vector for the jth wavelet
$\mathbf{m} = [m_{j,1}, \ldots, m_{j,p}]^T$ is dilation integer vector
$\mathbf{b}_j = b_0\mathbf{n}$ is the translation vector for the jth wavelet
$\mathbf{n} = [n_{j,1}, \ldots, n_{j,p}]^T$ is translation integer vector

Since the WNN equation (4.8) has the identical format as (4.1), it follows that the WNN can be uniquely determined by considering it as q MISO systems.

4.3 Multiresolution Signal Analysis

The theory of multiresolution signal decomposition of Mallat [40] provides the crucial framework for formulating and designing neural networks with wavelet activation functions. A recapitulation of these concepts as given in [40], [41], and [37] will now be presented.

A multiresolution signal analysis entails a sequence of successive closed approximation subspaces, V_m with $m \in \mathcal{Z}$, satisfying the following properties:

1. $$\cdots \subset V_2 \subset V_1 \subset V_0 \subset V_{-1} \subset V_{-2} \subset \cdots \tag{4.9}$$

2. $$\overline{\bigcup_{m \in \mathcal{Z}} V_m} = \mathcal{L}^2(I\!R) \tag{4.10}$$

3. $$\bigcap_{m \in \mathcal{Z}} V_m = \{\phi\} \tag{4.11}$$

4. $$f(x) \in V_m \iff f(2x) \in V_{m-1} \tag{4.12}$$

5. $$f(x) \in V_0 \implies f(x-j) \in V_0 \ \ \forall j \in \mathcal{Z} \tag{4.13}$$
   which due to (4.12) implies $f(x) \in V_m \implies f(x - 2^m j) \in V_m \ \ \forall j \in \mathcal{Z}$

6. There exists a scaling function $\phi \in V_0$ such that
   $$\{\phi_{0,j};\ j \in \mathcal{Z}\} \textit{ is an orthonormal basis in } V_0 \tag{4.14}$$
   with $\phi_{m,j}(x) = 2^{-m/2}\phi(2^{-m}x - j) \ \ \forall j, m \in \mathcal{Z}$

Equations (4.12) and (4.14) imply that $\{\phi_{m,j};\ j \in \mathcal{Z}\}$ is an orthonormal basis for $V_m \ \forall m \in \mathcal{Z}$. Define P_m to be the orthogonal projection operator onto V_m. By (4.10), $\lim_{m \Rightarrow -\infty} P_m f = f \ \ \forall f \in \mathcal{L}^2(I\!R)$. The crux of multiresolution analysis is that if a set

of closed subspaces satisfies (4.9) - (4.14), then there exists an orthonormal wavelet basis of $\mathcal{L}^2(\mathbb{R})$ given by:

$$\{\psi_{m,n};\ m,n \in \mathbb{Z}\}$$
$$\psi_{m,n}(x) = 2^{-m/2}\psi(2^{-m}x - n) \tag{4.15}$$

which for all $f \in \mathcal{L}^2(\mathbb{R})$ satisfies the relation

$$P_{m-1}f = P_m f + \sum_{n\in\mathbb{Z}} \langle f, \psi_{m,n}\rangle \psi_{m,n} \tag{4.16}$$

For every $m \in \mathbb{Z}$, define the orthogonal complement of V_m in V_{m-1} as W_m. At every scale

$$V_{m-1} = V_m \oplus W_m \tag{4.17}$$
$$W_m \perp W_{m'} \quad if\ m \neq m' \tag{4.18}$$
$$W_m \subset V_{m'} \quad if\ m > m' \tag{4.19}$$

Then, for $m < M$,

$$V_m = V_M \oplus \bigoplus_{i=0}^{M-m-1} W_{M-i} \tag{4.20}$$

From equations (4.10) and (4.11), it follows that $\mathcal{L}^2(\mathbb{R})$ can be decomposed into mutually orthogonal subspaces according to

$$\bigoplus_{m\in\mathbb{Z}} W_m = \mathcal{L}^2(\mathbb{R}) \tag{4.21}$$

Lastly, the W_m subspaces acquire the scaling property of equation (4.12):

$$f(x) \in W_m \iff f(2x) \in W_{m-1} \tag{4.22}$$

With the above definition for W_m, equation (4.16) equivalently states that $\{\psi_{m,n};\ m,n \in \mathbb{Z}\}$ is an orthonormal basis for W_m for fixed m. In addition, equation (4.22) guarantees that if $\{\psi_{0,n};\ n \in \mathbb{Z}\}$ is an orthonormal basis for W_0, then $\{\psi_{m,n};\ m,n \in \mathbb{Z}\}$ will also be an orthonormal basis for W_m, for any m.

The orthonormal basis constructed above using the multiresolution signal analysis, given by equation (4.15), is only valid for $\mathcal{L}^2(\mathbb{R})$. The easiest way of constructing an

orthonormal basis for $\mathcal{L}^2(\mathbb{R}^p)$ is to take the tensor product functions generated by p one dimensional wavelet bases:

$$\Psi_{m_1,n_1;m_2,n_2;\cdots;m_p,n_p}(x_1, x_2, \ldots, x_p) = \psi_{m_1,n_1}(x_1)\psi_{m_2,n_2}(x_2)\cdots\psi_{m_p,n_p}(x_p) \tag{4.23}$$

where $\{\Psi_{m_1,n_1;m_2,n_2;\cdots;m_p,n_p};\ \ m_i, n_i \in \mathbb{Z}\}$ is an orthonormal basis for $\mathcal{L}^2(\mathbb{R}^p)$. Another construction for multidimensional wavelets comes from performing a multidimensional multiresolution analysis in which the dilations of the resultant multidimensional wavelets control the p variables simultaneously [37]. However, multidimensional wavelets generated using either construction suffer from the drawback of depending on the dimension p of the input space [37]. The generation of nonseparable multidimensional wavelets appears to be a viable technique for overcoming the dependence of multidimensional wavelets on the dimension p of the input space [42].

4.4 Wavelet Neural Network Architecture 2

A second architecture for the wavelet network comes directly from a multiresolution signal analysis. Let $f_{m-1}(x)$ be the approximation of $f(x)$ at the $(m-1)$ scale. Then, since $f_{m-1}(x) \in V_{m-1}$ and recalling equation (4.17), it follows from equation (4.16) that,

$$f_{m-1}(x) = f_m(x) + \sum_{n\in\mathbb{Z}} d_{mn}\psi_{m,n}(x) \tag{4.24}$$

If $f(x) \approx f_{m-1}(x)$, i.e. the $(m-1)$ scale corresponds to the sampling rate of the function to be approximated, and recalling equation (4.14), then equation (4.24) becomes

$$f(x) \approx \sum_{n\in\mathbb{Z}} c_{Mn}\phi_{M,n}(x) + \sum_{i=m}^{M}\sum_{n\in\mathbb{Z}} d_{in}\psi_{i,n}(x) \tag{4.25}$$

Note from equations (4.14) and (4.12) that $f_M(x) = \sum_{n\in\mathbb{Z}} c_{Mn}\phi_{M,n}(x)$. The equation (4.25) was used in [43] to represent a wavelet neural network.

Now it should be clear that the wavelet neural network given by equation (4.8) can alternatively be represented by the mapping $y_{ik} : \mathbb{R}^p \to \mathbb{R}, \quad \forall i = 1, 2, \ldots, r$

$$y_{ik} = \lambda_{0k} + \sum_{l=1}^{M} \lambda_{lk}\ \phi(diag(\mathbf{a}_l)\mathbf{X}_i - \mathbf{b}_l) + \sum_{j=1}^{N} \lambda_{jk}\ \phi(diag(\mathbf{a}_j)\mathbf{X}_i - \mathbf{b}_j) \quad \forall k = 1, 2, \ldots, q \tag{4.26}$$

4.5 Wavelet Neural Networks

When developing a WNN, the primary design parameters to be determined consist of choosing appropriate translation vectors, $b_0\mathbf{n}$, and dilation factors, a_0^{-m}. This is equivalent to selecting kernel wavelets from the infinite set of candidate wavelets represented by

$$\{\psi_{m,n}(\mathbf{z}) = (det\mathbf{A})^{p/2}\psi(\mathbf{Az} - b_0\mathbf{n})\mathbf{m}, \mathbf{n} \in \mathbb{Z}^p\}, \mathbf{z} \in \mathbb{R}^p \tag{4.27}$$

where: $\mathbf{A} = diag(a0^{-m_1}, \ldots, a0^{-m_p})$. For multidimensional input spaces, there is an additional consideration of deciding how the multidimensional wavelets are to be generated. The separable multidimensional wavelets suffer from the drawback of being dependent on the dimension p of the input space. Another approach is to generate nonseparable multidimensional wavelets [42]. Alternately, a radial wavelet function can be used, which is defined by the mapping $\Psi : \mathbb{R}^+ \rightarrow \mathbb{R}$ [39]:

$$\psi(\mathbf{z}) = \Psi(\|\mathbf{z}\|_2) \tag{4.28}$$

Radial wavelets are not dependent on the dimension of the input space and are therefore better suited for large dimensional learning problems than direct product wavelets. Note that with radial wavelets the same dilation factor is used over each dimension of the input space, i.e., $diag(\mathbf{a}_j) = diag(a0^{-m_j}, \ldots, a0^{-m_j})$.

It has been shown that for appropriately chosen ψ, a_0, and b_0, equation (4.27) comprise frames of $\mathcal{L}^2(\mathbb{R}^p)$ [39]. The first step in selecting appropriate kernel wavelets is to truncate equation (4.27) into a finite set, which requires *a priori* knowledge about the given approximation problem. When ψ is chosen to be a radial wavelet, the truncated wavelet set can be denoted by

$$\{\psi_{m_j,n_j}(\mathbf{z}) = a_0^{-p\,m_j/2}\psi(a_0^{-m_j}\mathbf{z} - b_0\mathbf{n}_j) \quad m_j \in \overline{Z} \subset \mathbb{Z}, \mathbf{n}_j \in \tilde{Z} \subset \mathbb{Z}^p\} \tag{4.29}$$

Any truncated wavelet set should sufficiently cover the domain of the input vectors at the desired resolution level, m_j, while maintaining the position of the wavelets, $\mathbf{n}_j$, somewhere within the domain of the input vectors and allowing the support of the wavelets to extend beyond the range of the input training data. The truncated wavelet set, equation (4.29), has the form of a regular pyramid, see Figure 4.2, meaning that wavelets corresponding to the same dilation parameter are equally spaced/translated within the domain, and as the dilation parameter increases, the corresponding wavelets become denser/narrower within the domain. The parallels between the RBFNN and the WNN should now be apparent. Choosing the centroids, $\mathbf{C_j}$, for the RBFNN is equivalent to selecting the translation parameter vectors, $b_0\mathbf{n_j}$,

for the WNN. Similarly, choosing the smoothing factor(s), σ_j, for the RBFNN is equivalent to selecting the dilation parameter(s), $a_0^{-m_j}$, for the WNN. Thus, the OLS procedure [36] can be used on the truncated set of candidate wavelets equation (4.29) to determine the significant wavelets to within a specified tolerance ρ, $0 < \rho < 1$, [44]. The selection of the tolerance ρ is also the key to balancing the accuracy and complexity of the final WNN design.

4.6 Network Design

Figure 4.1 below shows the general architecture for the RBFNN and for the WNN.

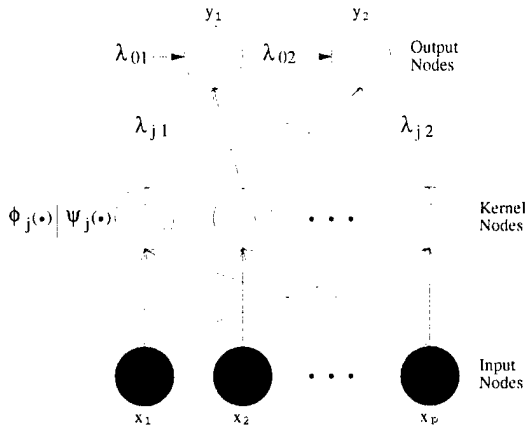

Figure 4.1: RBF and Wavelet NN Architecture for Learning

Once the training data has been determined, then the NN designs can be carried out. The kernel node activation function for the RBFNN (4.1) and the mother scaling activation function for the WNN when using the second architecture was selected to be a multivariate Gaussian function,

$$\phi(\mathbf{z}) = \exp\left(-\mathbf{z}^T\mathbf{z}\right);\ \mathbf{z} \in I\!R^p \tag{4.30}$$

The mother wavelet activation function for both architectures of the WNN (4.8) were selected to be the Laplacian of the multivariate Gaussian function, i.e. a radial wavelet,

$$\psi(\mathbf{z}) = \left(\frac{4\mathbf{z}^T\mathbf{z} - 2p\,\varsigma^2}{\varsigma^4}\right)\exp\left(-\frac{\mathbf{z}^T\mathbf{z}}{\varsigma^2}\right);\ \mathbf{z} \in I\!R^p \tag{4.31}$$

where ς represents the variance of the multivariate Gaussian. The development of the NNs involved a tradeoff between the complexity of the NNs and the resultant performance or accuracy of the NN interpolation.

Design Goal: Minimize the complexity of the NNs by keeping the number of kernel nodes to a minimum, while maintaining the normalized error below 5%.

For the RBFNN design, since a RBFNN with the same smoothing factor in each kernel node is capable of universal approximation [45], this characteristic should be exploited in order to simplify the number of design parameters to be determined. The initial smoothing factor can then be determined using a nearest neighbor criterion. Now the critical design parameters to be determined are the locations of the centroids for the kernel functions.

For the WNN design, a grid of the wavelets at the multiple resolution levels for each input range must be determined as shown in Figure 4.2. The wavelet coefficients a_0 and b_0 affect the alignment of the grid of wavelets for each input range. Since for appropriately chosen $a_0 > 1$ and $b_0 > 0$, radial wavelets comprise frames of $\mathcal{L}^2(\mathbb{R}^p)$ [39], it was decided to utilize this property in order to simplify the number of design parameters to be determined.

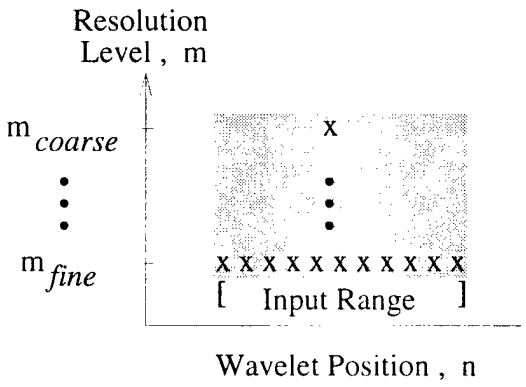

Figure 4.2: Grid of wavelets at multiple resolutions

In order to form the grid of wavelets for each input range, the minimum distance between data points for each input range needs to be determined, $\Delta x_{i,min}$. Then the finest resolution necessary for the grid over each input range is given by $a_0^{m_{i,fine}} = \Delta x_{i,min}$ which yields:

$$m_{i,fine} = round(\log_{a0} \Delta x_{i,min}) \tag{4.32}$$

The coarsest resolution for the grid over each input range, $m_{i,coarse}$, is determined by the largest value of m for which the first occurence of the smallest, nonzero number

of wavelets in the input range exists. Now the set of dilation integers for each input range is given by

$$\{m_{i,fine}, m_{i,fine}+1, \ldots, m_{i,coarse}\} = Z_i \subset \mathbb{Z} \tag{4.33}$$

Once the corresponding grid for each input range has been determined, then the multidimensional wavelets need to be generated. The use of radial wavelets greatly simplifies this task, since only those values of m common to all input ranges need to be considered. Recall that the same dilation factor is used over each dimension of the input space, $diag(\mathbf{a}_j) = diag(a0^{-m_j}, \ldots, a0^{-m_j})$, therefore

$$\overline{Z} = \bigcap_{i=1}^{p} Z_i \; ; \qquad with\ m_j \in \overline{Z} \subset \mathbb{Z} \tag{4.34}$$

Recall that radial wavelets have the added benefit of being independent of the dimension of the input space. Now, the corresponding set of translation integers for each common resolution level, m_j, is determined by

$$\begin{aligned} \mathbf{N}_{\mathbf{m}_j} &= \{round(\mathbf{X}_i/(a0^{m_j}b0)); i = 1, \ldots, r\} \\ \tilde{Z} &= \{\mathbf{N}_{\mathbf{m}_j} \ \forall m_j \in \overline{Z} \subset \mathbb{Z}\} \\ \mathbf{n}_j &\in \mathbf{N}_{\mathbf{m}_j} \subset \tilde{Z} \subset \mathbb{Z}^p \end{aligned} \tag{4.35}$$

Note that, for each m_j, there are $\mid \mathbf{N}_{\mathbf{m}_j} \mid$, (number of elements in the set $\mathbf{N}_{\mathbf{m}_j}$), corresponding $\mathbf{n}_j$ vectors. Then the truncated wavelet set, equation (4.29), is formed by using equations (4.34) and (4.35).

The design procedure utilized in developing RBF and wavelet NNs can be summarized for a given set of training data as follows:

1a. Select RBF function, $\phi(\mathbf{z})$. OR

1b. Select mother wavelet, $\psi(\mathbf{z})$, the scaling function $\phi(\mathbf{z})$ if using the second WNN architecture, and the dilation constant, a_0.

2a. Select the RBF smoothing factor, σ. OR

2b. Select the wavelet translation constant, b_0.

3a. Initialize the RBF centroids, $\mathbf{C_j} = \mathbf{X}_i$. OR

3b. Determine the set of wavelet dilation integers, $m_j \in \overline{Z}$, by generating a grid for each input range and then, for each m_j, find the set of translation integers, $\mathbf{n}_j \in \mathbf{N}_{\mathbf{m}_j} \subset \tilde{Z}$.

4. Choose the selection tolerance, ρ (typical 0.0001), and use OLS algorithm [36] to determine significant RBF centroids or wavelets from the truncated set.

5. Get least squares solution for weights, λ_{jk}.

6. Repeat above steps as necessary.

sectionNeural Network Modeling for Control Applications A RBFNN and a WNN will both be developed in order to model several actuator nonlinearities in a flexible structure. The purpose of the NNs will be to predict the dynamical characteristics of the actuator nonlinearity. A considerable amount of uncertainty exists in typical actuator nonlinearites. The output vector, $\mathbf{Y}_i = [\ y_{i1} \quad y_{i2}\ ]$, for the NNs consisted of:

1. Desired actuator torque.

Each training run was sampled at a rate of 10Hz for 500 seconds, resulting in 5001 data points. It was determined that a minimum of 6 training runs were necessary to evenly partition the input space, and these 6 training runs were selected as the preliminary set of training data. This preliminary set of training data contained 30,006 data points. Since the kernel node centroids are initially selected to correspond with the set of training data, the centroid selection procedure would have to be carried out over an initial number of 30,006 kernel nodes. As can be observed, the amount of computer memory and computational time necessary for even the minimal set of training data is exorbitant! Also, if additional training runs are deemed necessary, the size of the set of training data will only increase. One solution to the excessive data problem is to sample the training runs at a slower rate to reduce the number of data points down to a manageable number, and then test the performance of the resultant NN with the 10Hz set of training data. In theory, as long as the training data is chosen to be persistently exciting over the entire input space, retraining of the NNs, i.e. changing the kernel node to network output weights, will be unnecessary. In other words, the resultant NN performance with non-training set data should be comparable with its performance over the set of training data. Additional testing data not included in the training set was then used to measure the performance of the NNs.

4.7 RBF Neural Network Simulation Results

The RBFNN designs presented in this section follow the procedure outlined in Section 4.6 with only the smoothing factor, σ, being modified between designs. The initial smoothing factor for each kernel node was determined from the plot of the nearest neighbor distance versus training data vector index. The mean nearest neighbor distance is 0.98. Based on the nearest neighbor data, the initial smoothing factor was selected to be 1.0. Then the centroid selection procedure [36] was employed for a tolerance ρ of 0.0001. The selection procedure resulted in 260 kernel nodes being selected and an output bias. The main trends observed in the RBF designs were that the accuracy of the RBFNN near points of discontinuity decreases as σ increases and that the complexity of the resultant RBFNN tends to decrease as σ increases.

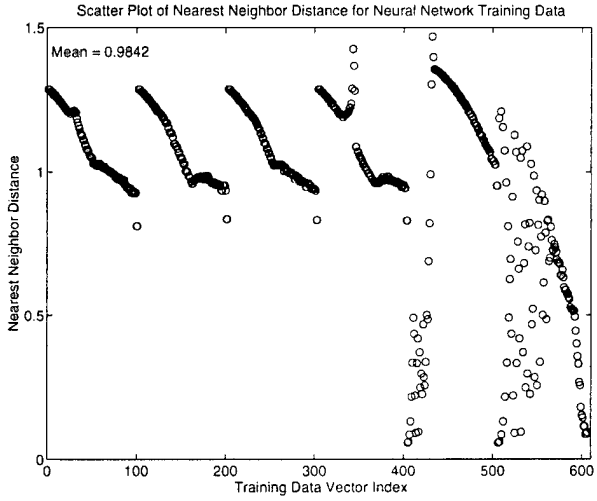

Figure 4.3: Scatter Plot of Nearest Neighbor Distance for NN Training Data

Table 4.1 summarizes the RBFNN designs discussed above in terms of the design parameter σ, the number of kernel nodes L, and the normalized error for each training vector of exemplars, E_k, given by equation ((4.36)) for the set of training vectors.

$$E_k = \sum_{i=1}^{r} \left(\frac{Y_i^* - Y_i}{Y_i^*} \right)^2 \tag{4.36}$$

where: E_k represents the normalized error
for the kth training vector
r is the number of exemplars
in each training vector
Y_i^* is desired output for ith exemplar

Y_i is the NN output for ith exemplar

σ	L	E_1	E_2	E_3	E_4	E_5	E_6
1.0	260	0.81	0.70	0.40	0.58	0.26	0.32
5.0	61	0.45	0.52	0.59	0.67	0.70	0.12
7.5	45	0.47	0.59	0.55	0.55	0.58	0.25
10	44	0.70	0.62	0.57	0.61	0.38	0.16
15	53	0.71	0.73	0.51	0.58	0.32	0.13
25	41	0.82	0.99	0.82	0.78	0.39	0.06

Table 4.1: RBFNN Training Design Summary

Table 4.2 compares designs 3 and 4 when tested using additional data not included in the training set.

σ	L	E_1	E_2	E_3	E_4	E_5	E_6
7.5	45	0.48	1.17	0.55	1.07	0.58	0.25
10	44	0.71	1.24	0.57	1.11	0.38	0.16

Table 4.2: RBFNN Testing Design Summary

Remark: If the normalized error was 5% at every point in a training run, $E_k = 250$. Therefore, the results shown in Tables 4.1 and 4.2 are excellent and more than satisfy the design goal stated in Section 4.6

The RBFNN output responses are given in Figures 4.4-4.6. Figures 4.4-4.6 compare the RBF output responses for design 4 with the actual set of testing data and provide the resultant error and normalized error responses. Observation of Figures 4.4-4.6 show that the performance is excellent and the goal of maintaining the normalized error below 5% everywhere except at an occasional point of discontinuity is satisfied.

4.8 Wavelet Neural Network Simulation Results

The WNN designs follow the procedure outlined in the Network Design Section with the translation constant, b_0, and the mother wavelet activation function, equation ((4.31)), being modified between designs. The mother wavelet was modified by varying the variance parameter, ς. Initially, $\varsigma = 1$. The dilation constant was set to $a_0 = 2$ and the initial translation constant was chosen as $b_0 = 1$. The resulting grid of wavelets for each input range is summarized below in Table 4.3, where $\mid N \mid$ denotes the number of elements in the set $\mathbf{N}_{\mathbf{m}_j}$.

x_1		x_2		x_3		x_4	
m_1	$\mid N \mid$	m_2	$\mid N \mid$	m_3	$\mid N \mid$	m_4	$\mid N \mid$
-7	1450	-7	1632	0	156	-7	52
-6	731	-6	832	1	78	-6	27
-5	366	-5	411	2	39	-5	14
-4	183	-4	207	3	21	-4	7
-3	92	-3	103	4	11	-3	4
-2	46	-2	53	5	5	-2	3
-1	24	-1	27	6	4	-1	2
0	12	0	13	7	2	0	1
1	7	1	7	8	1		
2	4	2	5				
3	3	3	3				
4	1	4	1				

Table 4.3: Grid of Wavelets for Actuator Data

From Table 4.3 it follows that $\overline{Z} = \{0\}$ and therefore $m_j = 0$. The set of translation integers, $\mathbf{n}_j \in \mathbf{N}_{\mathbf{m}_j}$, were determined using equation ((4.35)). Then the selection procedure [36] was employed for a tolerance ρ of 0.0001. The selection procedure resulted in 88 wavelets being selected and an output bias. The main trends observed in the wavelet designs were that the accuracy of the WNN increases as b_0 decreases and that the complexity of the resultant WNN tends to decrease as ς increases.

Table 4.4 summarizes the WNN designs discussed above in terms of the design parameters b_0 and ς, the number of kernel nodes L, and the normalized error for each training vector of exemplars, E_k, given by equation ((4.36)).

b_0	ς	L	E_1	E_2	E_3	E_4	E_5	E_6
1.0	1	88	11.4	5.72	58.2	50.1	13.5	1.35
0.5	1	245	0.81	0.58	0.53	0.70	0.34	0.32
0.1	1	242	0.71	0.62	0.51	0.76	0.48	0.39
0.5	4	104	0.46	0.63	0.45	0.65	0.94	0.10
0.5	10	48	0.51	0.74	0.41	0.62	0.52	0.18
0.1	10	46	0.55	0.61	0.45	0.66	0.54	0.24

Table 4.4: WNN Training Design Summary

Table 4.5 compares designs 5 and 6 when tested using additional data not included in the training set.

The results shown in Tables 4.4 and 4.5 are also excellent and more than satisfy the design goal. Comparison of Tables 4.2 and 4.5 demonstrates that the performance of the RBFNN and WNN are basically identical for this application. The WNN output

b_0	ς	L	E_1	E_2	E_3	E_4	E_5	E_6
0.5	10	48	0.52	1.35	0.40	1.05	0.52	0.18
0.1	10	46	0.56	1.20	0.45	1.08	0.54	0.24

Table 4.5: WNN Testing Design Summary

responses are given in Figures 4.7-4.9. Figures 4.7-4.9 compare the WNN output responses for design 6 with the actual set of testing data and provides the resultant error and normalized error responses. Observation of Figures 4.7-4.9 shows that the performance is excellent and the goal of maintaining the normalized error below 5% everywhere except at an occasional point of discontinuity is satisfied.

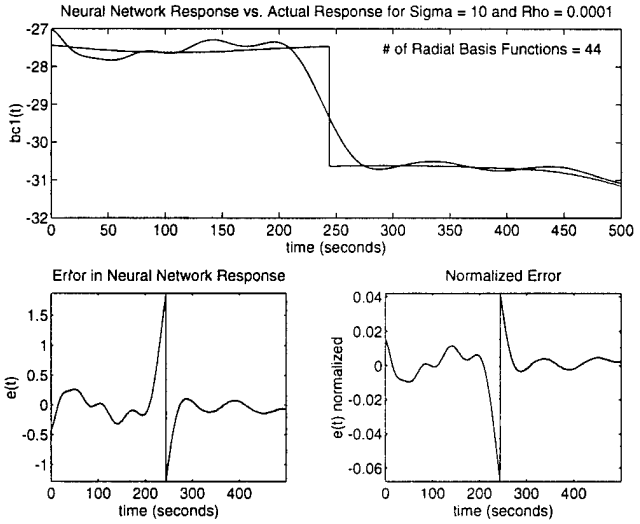

Figure 4.4: RBFNN Design 4 - Testing Run 1

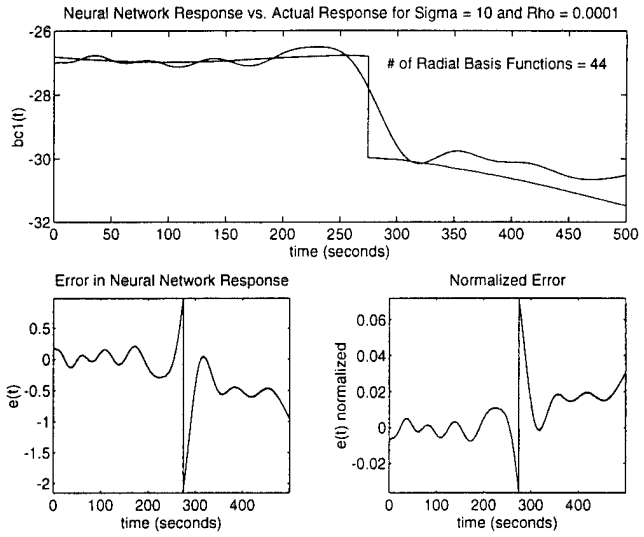

Figure 4.5: RBFNN Design 4 - Testing Run 2

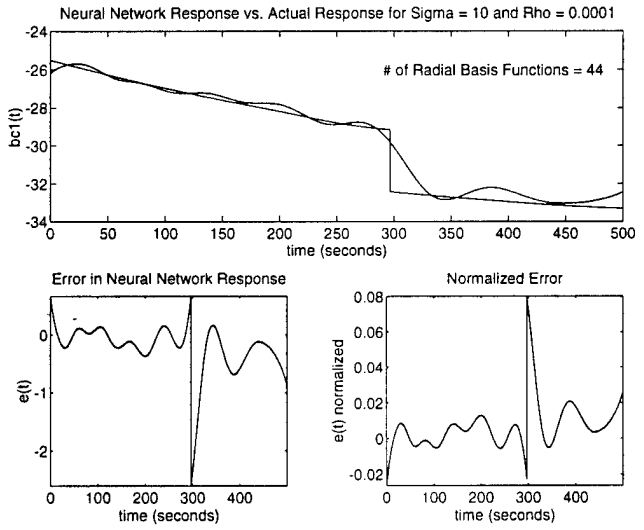

Figure 4.6: RBFNN Design 4 - Testing Run 4

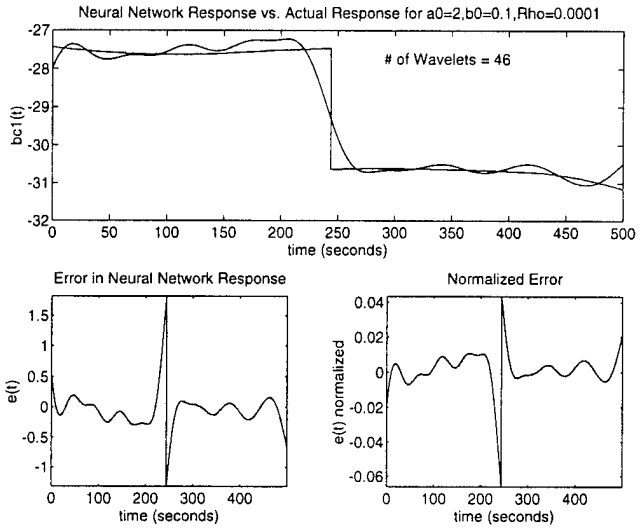

Figure 4.7: WNN Design 6 - Testing Run 1

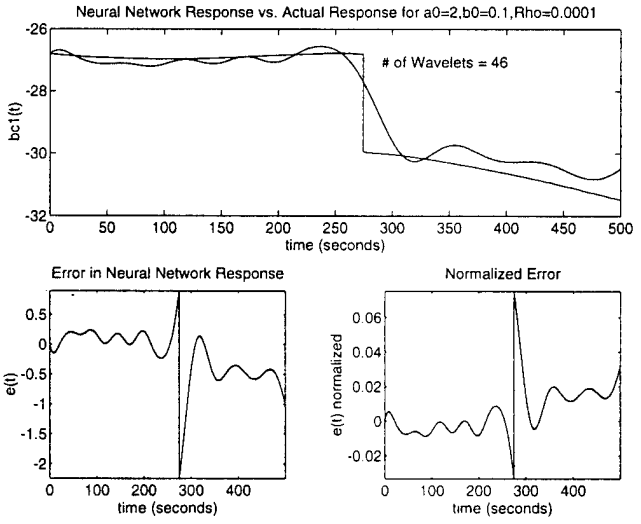

Figure 4.8: WNN Design 6 - Testing Run 2

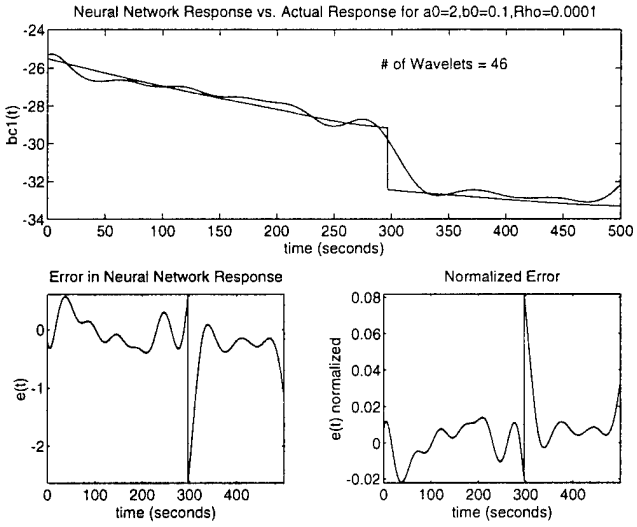

Figure 4.9: WNN Design 6 - Testing Run 4

5. MODELING AND CONTROL OF STRUCTURAL SYSTEMS USING WAVELETS

In this chapter, we explore a couple of uses for time-frequency wavelets. These include the modeling and control of structural systems and subsystems. We develop a versatile structure model based on time-frequency wavelets as opposed to the traditional finite element/modal models. The versatility of these wavelet models provides a means of developing a best basis for a given structural system. These wavelet models can be easily modified to account for structural changes due to the operating environment, coupled dynamic loading and material degradation. The wavelet models are developed for the purpose of being utilized during the controller design phase. We then present some theoretical results necessary for developing a sensitivity minimization controller based on a wavelet model. The theoretical work for other controller objectives can also be performed as extensions of this work. Initial proof of concept studies will be performed on several flexible structure models using simulation.

The main concept presented in this chapter is to use a wavelet basis to model the structural system and then determine the optimal controller using this same wavelet basis in an effort to obtain a nesting property between controllers of different order. The nesting property which wavelets possess is one of their primary strengths. The control problem to be addressed is that of minimizing the effect of disturbances on a SISO closed loop system, i.e., minimizing the sensitivity function, in terms of the H^2 norm. This control problem solution will be discussed herein and appeared in [46]. The time/space localization property of wavelets provides for the capability of "localized" control action over a selected period of time. This type of control should prove invaluable for structural systems with stringent positional or pointing requirements.

Wavelets provide a rich theory with a library of functions and algorithms available for modeling signals. Wavelets also have the ability to attain a best basis for a signal or class of signals. This means that a best basis of wavelet functions can be easily modified to account for uncertainties, failures, and changes in the operating environment of a structural system by simply changing the coefficients on the wavelet basis functions. Since wavelet coefficients tend to decay quickly and usually require substantially fewer basis functions compared with a Fourier basis, truncation of an infinite dimensional wavelet model to a finite dimensional model should introduce negligible modeling error. In addition, if the controller also depended on the same wavelet basis functions as the structural system, then the controller could also be easily modified to account for uncertainties, changes in operating environment of the structure, etc., making for a more robust controller.

5.1 Background on Time-Frequency Wavelets

There are many excellent articles and books on general wavelet theory, for example, see [37], [47], [48], [49], [40], [50] and [41] and the references therein. Wavelets are a set of basis functions, $\psi_{m,n}(x)$ which can be used to represent all admissible functions $f(x) \in \mathcal{H}$, Hilbert space, as follows:

$$f(x) = \sum_{m,n} c_{m,n}\psi_{m,n}(x) \tag{5.1}$$

The interesting characteristic of wavelets is that the basis functions, $\psi_{m,n}(x)$, are constructed from dilations and translations of a mother wavelet, $\psi(x)$. Time-frequency wavelets are closely linked to the Short Time Fourier Transform (STFT) which was pioneered by Gabor [51]. However, "Gabor" wavelets suffer from serious algorithmic difficulties and can never be an orthonormal basis for $\mathcal{L}^2(\mathbb{R})$. A significant improvement over the "Gabor" wavelets has been the development of orthogonal time-frequency wavelets by Coifman and Meyer [52], and Malvar [53, 54]. These researchers use smooth window functions to split the signal and employ extension concepts from the discrete cosine transform (DCT-IV) to "fold" the overlapping parts back into the split signal. Their clever construction allows one to construct smooth orthonormal bases for $\mathcal{L}^2(\mathbb{R})$ which depend on arbitrary partitions of the real line [55], [48], [49].

The following definitions are essential to understanding the construction of orthonormal time-frequency wavelets. Some of these definitions can be found in Wickerhauser, [48].

Definition 2 (Function Polarity) *A function f has positive polarity (+) with respect to the point α on the interval $[a-\epsilon, a+\epsilon] \iff f(t) = f(2a-t)$ for $t \in [a-e, a+e]$. In other words, f is an even function about the point a. A function f has negative polarity (-) with respect to the point a on the interval $[a-\epsilon, a+\epsilon] \iff f(t) = -f(2a-t)$ for $t \in [a-e, a+e]$. In other words, f is an odd function about the point a.*

Definition 3 (Cutoff Functions) *A cutoff function, $m(t) \in \mathcal{C}^d(\mathbb{R})$, is a complex, continuous, d-times differentiable function with the following properties:*

- $|m(t)|^2 + |m(-t)|^2 = 1 \ \ \forall t \in \mathbb{R}$
- $m(t) = \begin{cases} 0, & if \ \ t \leq -1, \\ 1, & if \ \ t \geq 1. \end{cases}$

Definition 4 (Bell Function) *A bell function, $b_j(t)$, supported on the interval $[a_j - e_j, a_{j+1} + e_{j+1}]$ is given by:*

$$b_j(t) = \begin{cases} m_j\left(\frac{t-a_j}{e_j}\right), & t \in [a_j - e_j, aj + e_j] \\ 1, & t \in [a_j + e_j, a_{j+1} - e_{j+1}] \\ m_{j+1}\left(\frac{a_{j+1}-t}{e_{j+1}}\right), & t \in [a_{j+1} - e_{j+1}, a_{j+1} + e_{j+1}] \end{cases}$$

Definition 5 (Folding Operator) *The folding operator, F, is given by:*

$$F(m)g(t) = \begin{cases} \bar{m}(\frac{a_j-t}{e_j})g(t) - \bar{m}(\frac{t-a_j}{e_j})g(2a_j - t), & if \;\; a_j - e_j < t < a_j \\ m(\frac{t-a_j}{e_j})g(t) + m(\frac{a_j-t}{e_j})g(2a_j - t), & if \;\; a_j < t < a_j + e_j, \\ g(t), & otherwise \end{cases}$$

Definition 6 (Unfolding Operator) *The adjoint of the folding operator, F^* the unfolding operator, is given by:*

$$F^*(m)g(t) = \begin{cases} m(\frac{a_j-t}{e_j})g(t) + \bar{m}(\frac{t-a_j}{e_j})g(2a_j - t), & if \;\; a_j - e_j < t < a_j \\ \bar{m}(\frac{t-a_j}{e_j})g(t) - m(\frac{a_j-t}{e_j})g(2a_j - t), & if \;\; a_j < t < a_j + e_j, \\ g(t), & otherwise \end{cases}$$

Unitary Operator Property: $F^*(m)F(m)g(t) = F(m)F^*(m)g(t) \;\; \forall t \neq a_j$
Action Interval: $[a_j - e_j, a_j + e_j]$

Definition 7 (Translation Operator) *The translation operator is given by:*
$S_a g(t) = g(t - a)$
The adjoint of the translation operator is given by:
$S_a^* g(t) = g(t + a)$

Definition 8 (Dilation Operator) *The dilation operator is given by:* $D_e g(t) = e^{-1/2} g(t/e)$
The adjoint of the dilation operator is given by: $D_a^* g(t) = e^{1/2} g(et)$

The translation and dilation operators can now be used to make the action region of the folding and unfolding operators the interval (a-e,a+e) as follows:

$$F(m_k, a_k, e_k)g(t) = S_{a_k} D_{e_k} F \; D_{e_k}^* S_{a_k}^* g(t)$$

$$= \begin{cases} \bar{m_k}(\frac{a_k-t}{e_k})g(t) - \bar{m_k}(\frac{t-a_k}{e_k})g(2a_k - t), & if \;\; a_k - e_k < t < a_k \\ m_k(\frac{t-a_k}{e_k})g(t) + m_k(\frac{a_k-t}{e_k})g(2a_k - t), & if \;\; a_k < t < a_k + e_k, \\ g(t), & otherwise. \end{cases} \tag{5.2}$$

$$F^*(m_k, a_k, e_k)g(t) = S_{a_k} D_{e_k} F^* \; D^*_{e_k} S^*_{a_k} g(t)$$

$$= \begin{cases} m_k(\frac{a_k - t}{e_k})g(t) + \bar{m}_k(\frac{t - a_k}{e_k})g(2a_k - t), & if \;\; a_k - e_k < t < a_k \\ \bar{m}_k(\frac{t - a_k}{e_k})g(t) - m(\frac{a_k - t}{e_k})g(2a_k - t), & if \;\; a_k < t < a_k + e_k, \\ g(t), & otherwise. \end{cases} \tag{5.3}$$

Notation: Let $F(m_k, a_k, e_k) = F_k$ and $F^*(m_k, a_k, e_k) = F^*_k$.

Definition 9 (Disjoint Folding Operators) *A family of folding $\{F_k\}$ and unfolding $\{F^*_k\}$ operators is disjoint, and therefore commutes, if* $(a_k - e_k, a_k + e_k) \bigcap (a_{k+1} - e_{k+1}, a_{k+1} + e_{k+1}) = \emptyset$.

Now, the real line, $\mathbb{R}$, is partitioned into compatible, disjoint intervals, $\mathbb{R} = \bigcup_k I_k$ and $\bigcap_k I_k = \emptyset$ as follows:
Let $\{c_k : k \in \mathbb{Z}\}$ be any sequence such that

- For $k < j$, $c_k < c_j$
- $c_k \to \infty$ and $c_{-k} \to -\infty$ as $k \to \infty$

For each $k \in \mathbb{Z}$, define:

$$a_k = \frac{1}{2}[c_k + c_{k+1}] \tag{5.4}$$

$$e_k = \frac{1}{2}[c_{k+1} - c_k] \tag{5.5}$$

$$I_k = [a_k, a_{k+1}] \tag{5.6}$$

Figure 5.1 shows how the intervals for the trigonometric basis are partitioned and demonstrates that any given interval I_k is only overlapped by the intervals I_{k-1} and I_{k+1}. Figure 5.1 also demonstrates that the midpoint of the kth interval, I_k, is c_{k+1}.

This partition can then be refined by splitting the intervals at their midpoints. For the jth refinement level, the intervals are given by:

$$I_{j,k} := \left[\frac{a_k}{2^j}, \frac{a_{k+1}}{2^j}\right] \tag{5.7}$$

The development of local trigonometric transforms which serve as a complete orthonormal basis for $\mathcal{L}^2(\mathbb{R})$ hinges on the properties of the bell functions, the definitions of the folding and unfolding operators, and the polarity of trigonometric

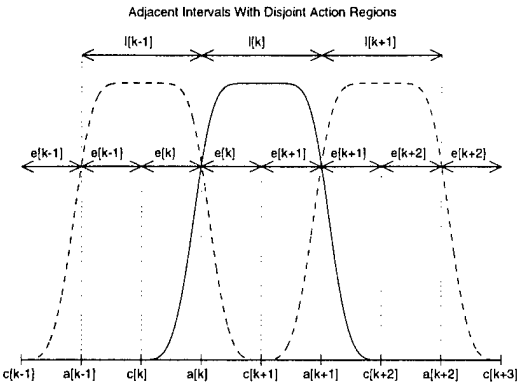

Figure 5.1: Partition of intervals, $\{I_k\}$, constructed using disjoint action regions at the interval endpoints

transform used. Two examples of complete, orthonormal local trigonometric bases are the Local Cosine Transform of Type IV (LCT-IV) and the Local Sine Transform of Type IV (LST-IV). When the bells $b_j(t)$ are symmetric with respect to their centers, i.e., $e_j = e_{j+1} \quad \forall j$, and the same cutoff function is used throughout, i.e., $m_j(t) = m_{j+1}(t) \quad \forall j$, the interval $I = (a_k, a_{k+1})$ is compatible with its adjacent translate by $|I| = a_{k+1} - a_k$. For this special case, the folding and unfolding operators simplify as follows:

Definition 10 (Folding Operator for Compatible Intervals) *The folding operator for compatible intervals, FC, is given by:*

$$FC(m)g(t) = \begin{cases} m(\frac{t-a_j}{e})g(t) + m(\frac{a_j-t}{e})g(a_j + a_{j+1} - t), & if \quad a_j < t < a_j + e, \\ \bar{m}(\frac{a_{j+1}-t}{e})g(t) - \bar{m}(\frac{t-a_{j+1}}{e})g(a_j + a_{j+1} - t), & if \quad a_{j+1} - e < t < a_{j+1} \\ g(t), & otherwise \end{cases}$$

Definition 11 (Unfolding Operator for Compatible Intervals) *The unfolding operator for compatible intervals, FC^*, is given by:*

$$FC^*(m)g(t) = \begin{cases} \bar{m}(\frac{t-a_j}{e})g(t) - m(\frac{a_j-t}{e})g(a_j + a_{j+1} - t), & if \quad a_j < t < a_j + e, \\ m(\frac{a_{j+1}-t}{e})g(t) + \bar{m}(\frac{t-a_{j+1}}{e})g(a_j + a_{j+1} - t), & if \quad a_{j+1} - e < t < a_{j+1} \\ g(t), & otherwise \end{cases}$$

With the use of these compatible interval folding and unfolding operators, there is no longer any need to step outside of the interval when performing folding and unfolding.

The general form of a typical family of time-frequency wavelets is given by:

$$\psi_{n,k}(t) = F_k^* F_{k+1}^* \chi_{I_k}(t) \cos_{n,k}(t) = \sqrt{\frac{2}{|I_k|}} w_k(t) \cos\left(\frac{\pi\left(n+\frac{1}{2}\right)(t-a_k)}{|I_k|}\right) \qquad (5.8)$$

where: $\psi_{n,k}(t) \in L^2(\mathbb{R})$

$\chi_{I_k}(t) = \chi(\frac{t-a_k}{e_k}) = \begin{cases} 1, & if \ \ a_k \leq t \leq a_{k+1}, \\ 0, & otherwise. \end{cases}$

$\cos_{n,k}(t) = \sqrt{\frac{2}{|I_k|}} \cos\left(\frac{\pi\left(n+\frac{1}{2}\right)(t-a_k)}{|I_k|}\right)$

$w_k(t) = m_k\left(\frac{t-a_k}{e_k}\right) m_{k+1}\left(\frac{a_{k+1}t}{e_k}\right)$, $Supp\ w_k(t) = [a_k - e_k, a_{k+1} + e_{k+1}]$

$I_k = [a_k, a_{k+1}]$ is the kth interval

$|I_k| = a_{k+1} - a_k$

The time-frequency wavelets allow for windows of varying length in which the time domain is divided into unequal intervals. Figure 5.2 shows a typical time-frequency wavelet.

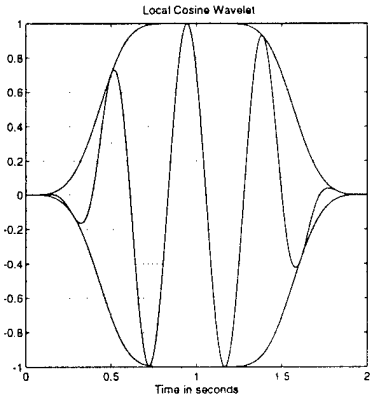

Figure 5.2: Typical Time-Frequency Wavelet

Properties of $\psi_{n,k}(t)$:

(i) Orthonormality: $\langle \psi_{n,k}(t), \psi_{m,j}(t) \rangle = \delta_{n,m}\delta_{k,j}$.

(ii) Compact Support: $Supp\ \psi_{n,k}(t) = [a_k - e_k, a_{k+1} + e_{k+1}] \Longrightarrow \psi_{n,k}(t) \in L^1(\mathbb{R})$.

(iii) Minimal Overlap: For a given interval, I_k, $\psi_{n,k}(t)$ is only overlapped by $\psi_{n,k-1}(t)$ and $\psi_{n,k+1}(t)$ due to being constructed from disjoint folding and unfolding operators.

Remark

The construction of disjoint intervals for $I\!R(0,\infty)$ requires that $c_{-k} \rightarrow 0$ as $k \rightarrow \infty$. Such a partition yields a continuous, orthonormal local trigonometric basis for $L^2(0,\infty)$ [55]. Now, for appropriately selected cutoff functions, an orthonormal H^2 wavelet basis can be determined by taking the Laplace transform of each element in this basis for $L^2(0,\infty)$.

5.2 Structural System Modeling and Identification

The control of advanced structural systems is a demanding task due mainly to the intrinsic dynamic characteristics of these structures. Typical modeling approaches involve using structural analysis programs like NASTRAN for developing finite element models [56, 57]. Typically, finite element models can be characterized by the presence of densely packed modal frequencies with low damping [58]. In addition, finite element models do not account for the many uncertainties present in the structure, including structural uncertainties, failure of system components, and changes in the operating environment. For a 1% error in the dominant modal frequency, the modeling error could be as large as the contribution of the mode itself [59]. Truncation and round off inherent in using a finite-dimensional model for an infinite dimensional system invariable introduce additional errors in the modal frequencies and the mode shapes. Lastly, different modes may be excited during different operating/failure conditions requiring a versatile model of the structure.

A general SISO structural plant model can be represented as:

$$P(s) = \sum_{k=0}^{\infty} \frac{g_k}{s^2 + 2\zeta k\omega_k s + \omega_k^2} \tag{5.9}$$

where g_k is a gain term. Assume that any rigid body modes have been stabilized by an inner loop. Then P(s) $\in H^2$. The structural plant, P(s), can now be modeled by using a time-frequency wavelet representation of the form:

$$P(s) = \sum_{k=0}^{\infty} \alpha_k \Psi_{n_k,k}(s) \tag{5.10}$$

where $\Psi_{n_k,k}(s)$ is an H^2 wavelet basis function. Due to the linearity of the Fourier Transform, and the fact that the Fourier Transform is an isomorphism between $L^2[0,\infty)$ and H^2, the equivalent time domain representation of structural system is given by:

$$p(t) = \sum_{k=0}^{\infty} \alpha_k \psi_{n_k,k}(t) \tag{5.11}$$

where $\psi_{n_k,k}(t) \in L^2(0,\infty) \bigcap L^1(0,\infty)$.

The control designer would like to be able to obtain a best basis for a given structural system, or possibly a best basis (BB) for a class of structural systems / subsystems. A best basis selection algorithm [60], based on a signal processing viewpoint, has already been developed. The BB selection procedure is an adaptive algorithm which determines the splitting locations for the time-frequency wavelets based on the signal to be decomposed. The decision is based on yielding a representation which has the most decorrelation. Entropy is one method out of many possible methods, [48], used to measure the decorrelation. There are also many other adaptive techniques which can be utilized in the selection of the best basis for a given signal. It should be noted that for the controller design presented herein, the BB selection procedure would have to be modified to ensure that the basis elements selected remain orthogonal to each other. Another possible approach is to determine the best level basis out of the total number of depth levels considered for the given structural system. This best level basis could serve as the structural basis and would maintain the required orthogonality between the basis elements. Figure 5.3 provides an example of possible splitting locations for a time-frequency wavelet representation of a particular signal and then gives a potential orthogonal basis and a potential level basis, which by definition is guaranteed to be orthogonal.

Figure 5.4 outlines the procedure for the decomposition of a particular discrete signal, $x(k)$, into cosine packets (Cosine Packet Analysis) and the procedure for the reconstruction of the discrete signal from the cosine packets (Cosine Packet Synthesis). Figure 5.4 demonstrates these procedures for a given depth level, d, in the packet table, corresponding to a level basis analysis/synthesis procedure. Note that DCT-IV denotes the discrete cosine transform of type IV. It should be noted that sine packets, using the discrete sine transform of type IV (DST-IV), or a combination of both sine and cosine packets can also be used.

Figures 5.5 - 5.7 presents an example of a time-frequency wavelet decomposition, in particular, the cosine packet decomposition, basis selection, and cosine packet reconstruction of the impulse response for a structural system containing two modes. The basis to be determined was the best basis for the system with entropy as the information cost function to be minimized by the basis selection procedure.

Figures 5.8 - 5.10 presents the same example of the cosine packet decomposition, etc., as figures 5.5 - 5.7, but the basis to be determined is the best level basis for the system with entropy as the information cost function.

5.3 Multiresolutional Sensitivity Minimization

The feedback control system is shown in Figure 5.11, where P is the plant to be controlled and W is the weight modeling the disturbances. The Wiener-Hopf approach to the sensitivity minimization problem involves finding an internally stabilizing controller, C, such that the following performance is achieved:

$$\mu := \inf_{C \text{ stabilizing } P} \|WS\|_2 \tag{5.12}$$

The sensitivity function for the feedback control system is given by:

$$S := (1 + PC)^{-1} \tag{5.13}$$

The sensitivity minimization problem has been studied by numerous researchers in terms of minimizing the H^2 norm and the H^∞ norm, see [61], [62] and [63] and the references contained therein.

Assumptions

1. $W \in I\!RH^2$, i.e., W is real, rational, stable and strictly proper.
2. $P \in H^2$, i.e., P is stable.

The first step in our MC development is to perform a Youla parameterization [64] for the controller C according to:

$$C = Q(1 - PQ)^{-1}, \quad Q \in H^\infty, \quad (1 - PQ) \neq 0 \tag{5.14}$$

The performance measure, equation (5.12), becomes

$$\mu = \inf_{Q \in H^\infty} \|W(1 - PQ)\|_2 \tag{5.15}$$

$$\mu = \inf_{\hat{Q} \in H^2} \|W - P\hat{Q})\|_2 \tag{5.16}$$

where: $\hat{Q} = WQ$
Now represent the performance criteria, equation (5.16), as an binner product:

$$J = \|W - P\hat{Q}\|_2^2 = \langle W - P\hat{Q}, W - P\hat{Q} \rangle$$

$$= \langle W, W \rangle - 2Re\{\langle W, P\hat{Q} \rangle\} + \langle P\hat{Q}, P\hat{Q} \rangle \tag{5.17}$$

Let the Fourier Transform of a signal $x(t)$ be represented by $X(j\omega)$ and recall the following theorem:

Theorem 8 (Plancherel) *If $f(t) \in L^2(\mathbb{R})$, then $F(j\omega) \in L^2(j\mathbb{R})$ and $\|f\| = \|F\|$. In addition, $\langle f, g \rangle = \langle F, G \rangle$ for any two functions $f, g \in L^2(\mathbb{R})$.*

In light of this theorem, the performance criteria, J, can be represented equivalently as:

$$J = \langle w, w \rangle - 2Re\{\langle w, p\hat{q} \rangle\} + \langle p\hat{q}, p\hat{q} \rangle \tag{5.18}$$

The next step in our MC development is to represent the plant P using an orthonormal, preferably best, H^2 wavelet basis according to equation (5.10) given previously. Now, the disturbance weight W, and the controller function $\hat{Q}$ will also be represented by the same orthonormal, H^2 wavelet basis as follows:

$$W(s) = \sum_{k=0}^{\infty} \beta_k \Psi_{n_k,k}(s) \tag{5.19}$$

$$\hat{Q}(s) = \sum_{k=0}^{\infty} \gamma_k \Psi_{n_k,k}(s) \tag{5.20}$$

The equivalent time domain representation of these signals is given by:

$$w(t) = \sum_{k=0}^{\infty} \beta_k \psi_{n_k,k}(t) \tag{5.21}$$

$$\hat{q}(t) = \sum_{k=0}^{\infty} \gamma_k \psi_{n_k,k}(t) \tag{5.22}$$

Define:

$$\Gamma := [\gamma_0 \gamma_1 \gamma_2 \cdots]^T . \tag{5.23}$$

The performance measure is to be minimized by choosing the optimal gains, Γ, for the controller function $\hat{Q}$. However, due to the local nature of the wavelet basis functions used to represent the components of the system, the performance measure, equation (5.18), can be written as:

$$J(\Gamma) = \sum_{I_k} J_k(\gamma_k) \tag{5.24}$$

Making use of equation (5.24) and Figure 5.1 of Section 5.1, the optimal controller gains, Γ^{opt}, are determined. The complete derivation is presented in [46]. The optimal controller gain for a given interval, k, can be represented functionally as:

$$\gamma_k = f(\alpha_{k-1}, \alpha_k, \alpha_{k+1}, \beta_{k-1}, \beta_k, \beta_{k+1}, \psi_{k-1}, \psi_k, \psi_{k+1}, \gamma_{k-1}, \gamma_{k+1}) \tag{5.25}$$

5.4 Multiresolutional Controller Development and Implementation

The theoretical development of a multiresolutional controller for sensitivity minimization was presented in Section 5.3. The section discusses some of the implementation issues prevalent to the design of a multiresolutional controller (MC) for sensitivity minimization. First, the functional representation of the controller gains, γ_k, found in equation (5.25), actually represents inner product terms of the time-frequency wavelets, $\psi_k(t)$, which can be evaluated numerically using equation (5.8) and the unitary operator property of the folding operators, see Definition 5, as follows:

$$\langle f, \psi_{n,k}(t) \rangle = \langle f, F_k^* F_{k+1}^* \chi_{I_k}(t) \cos_{n,k}(t) \rangle$$

$$= \langle F_{k+1} F_k f, \chi_{I_k}(t) \cos_{n,k}(t) \rangle \tag{5.26}$$

Secondly, the optimal controller gains are a function of the best basis chosen for the plant. Therefore, the controller design is extremely problem and plant specific. This is by no means a drawback, and actually is exactly what a control designer would want. However, a suboptimal controller should be directly related to the optimal controller when represented using a wavelet basis. Determining the optimal algorithm to use for the selection of the best wavelet basis functions also needs to be addressed. However, the best basis selection algorithm [60] appears to be a good starting place, keeping in mind that the resultant best basis must be orthogonal so that the controller methodology developed is applicable. Next is the need to truncate the infinite wavelet basis representation for the plant. Again, this is not a drawback, but a feature of wavelets that is usually exploited, especially in video compression problems. Wavelets are such a powerful tool since they require less basis functions than the standard Fourier methods due to their localization in both time and frequency. Another issue is selection of the best optimization technique to use when solving equation (5.25) for the optimal γ_k's. Due to the coupling between the γ_k, γ_{k-1} and γ_{k+1} terms, a recursive solution is possible which would relate the first γ gain to the last γ gain, and then all the intermediate gains would be found by back substitution. Other optimization procedures could also be employed, possibly a dynamic programming method starting at the last time interval or a conjugate gradient procedure. Lastly, suboptimal γ_k's could always be calculated by simply calculating bounds on the cross coupling terms,

and using these bounds in the calculation for the γ_k's. Then the optimization problem is directly solved by determining the γ_k gains, for all k = 0,1, ..., N, using equation (5.25).

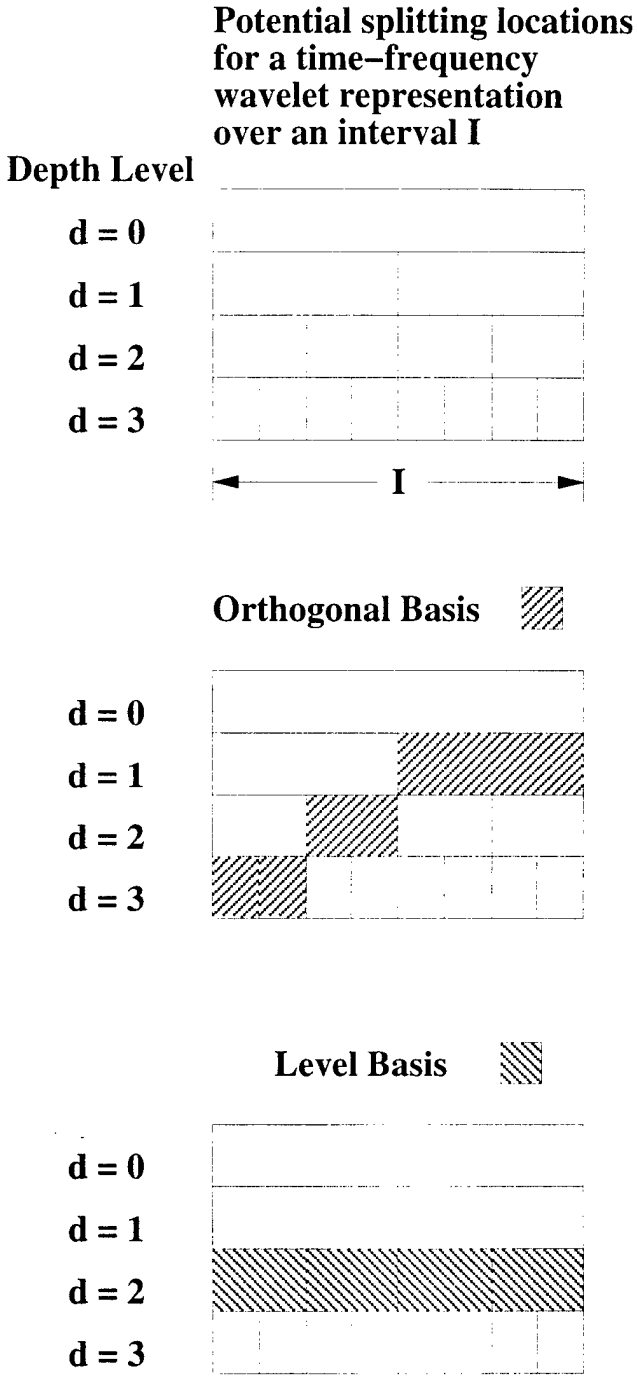

Figure 5.3: Example of possible splitting locations for a particular signal and a potential orthogonal basis and a potential level basis

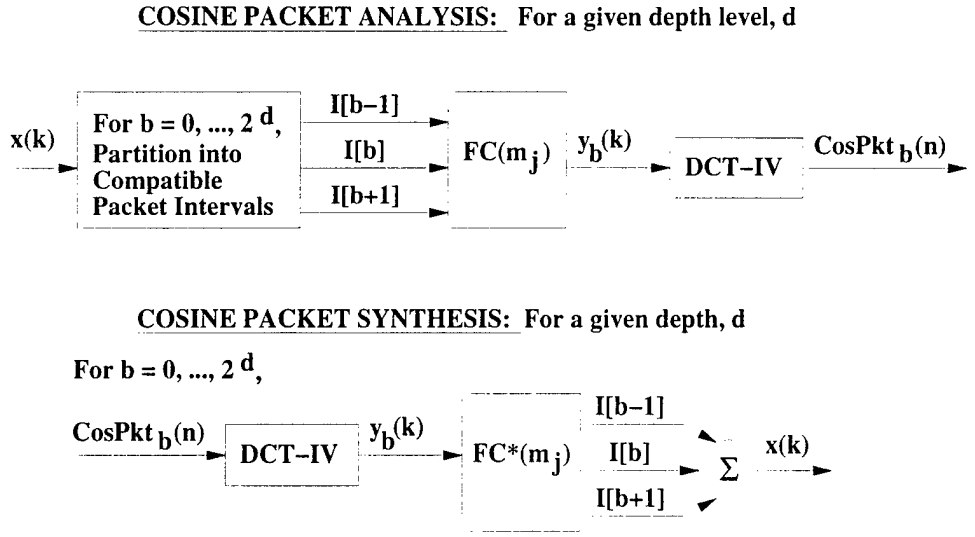

Figure 5.4: Procedures for performing cosine packet analysis and synthesis on a discrete signal, $x(k)$, for a particular depth level, d.

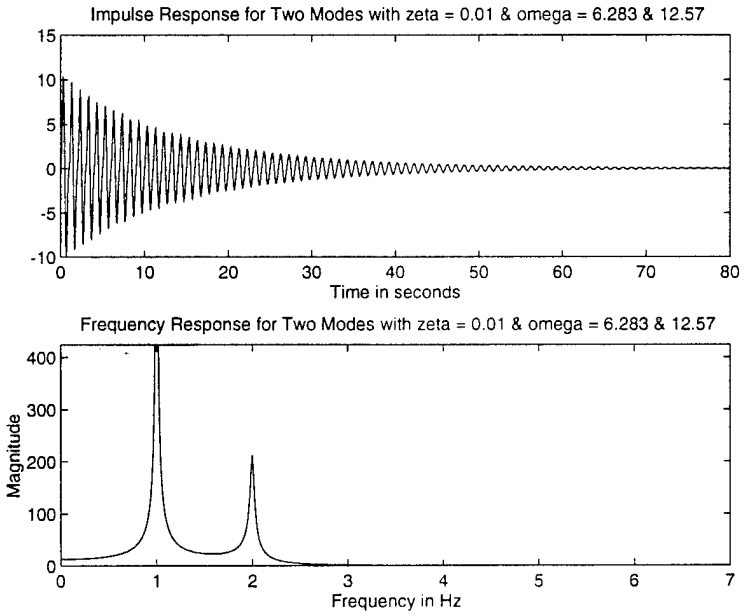

Figure 5.5: Impulse and frequency response for a flexible structure with two modes

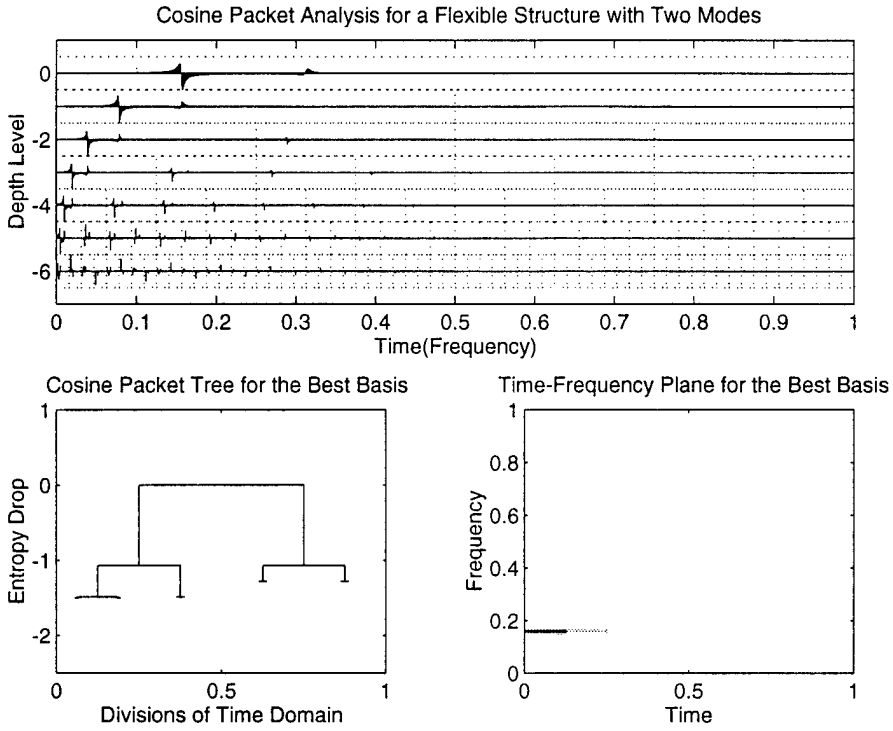

Figure 5.6: Cosine packet decomposition and best basis selection for a flexible structure with two modes at $\omega_1 = 2\pi$ and $\omega_2 = 4\pi$ with the identical damping factor of $\zeta = 0.01$.

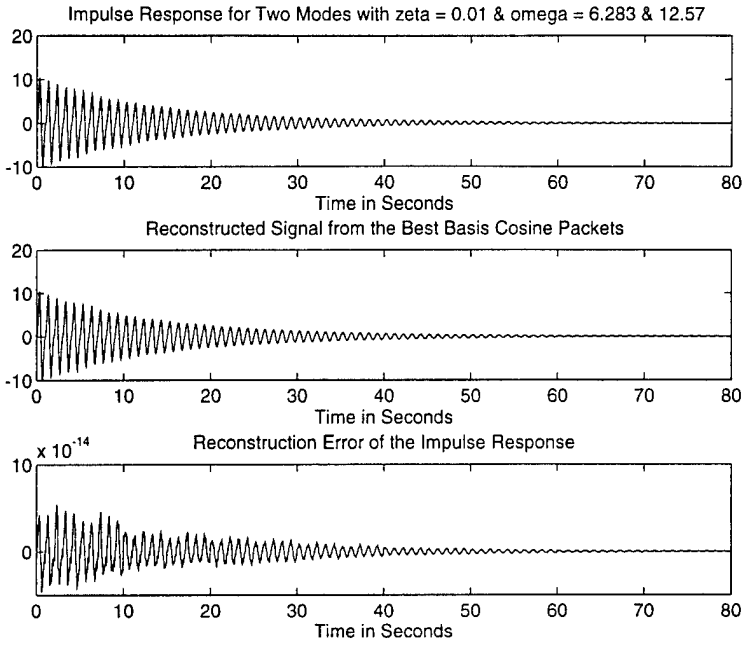

Figure 5.7: Reconstruction of the impulse response for a flexible structure with two modes

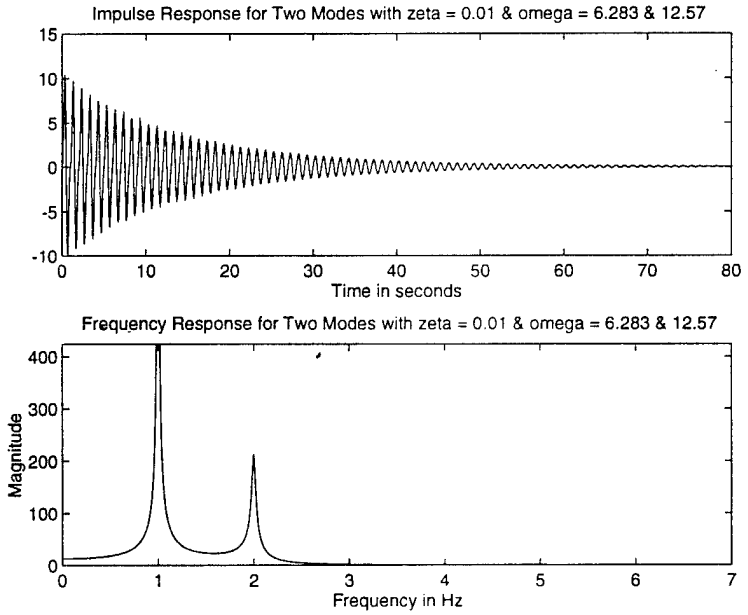

Figure 5.8: Impulse and frequency response for a flexible structure with two modes

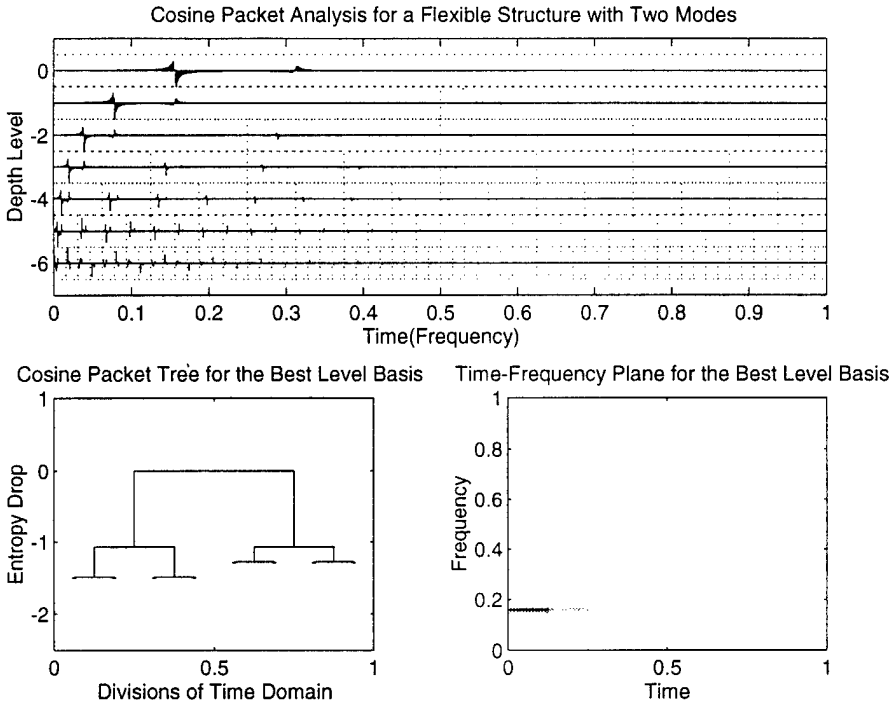

Figure 5.9: Cosine packet decomposition and best level basis selection for a flexible structure with two modes at $\omega_1 = 2\pi$ and $\omega_2 = 4\pi$ with the identical damping factor of $\zeta = 0.01$.

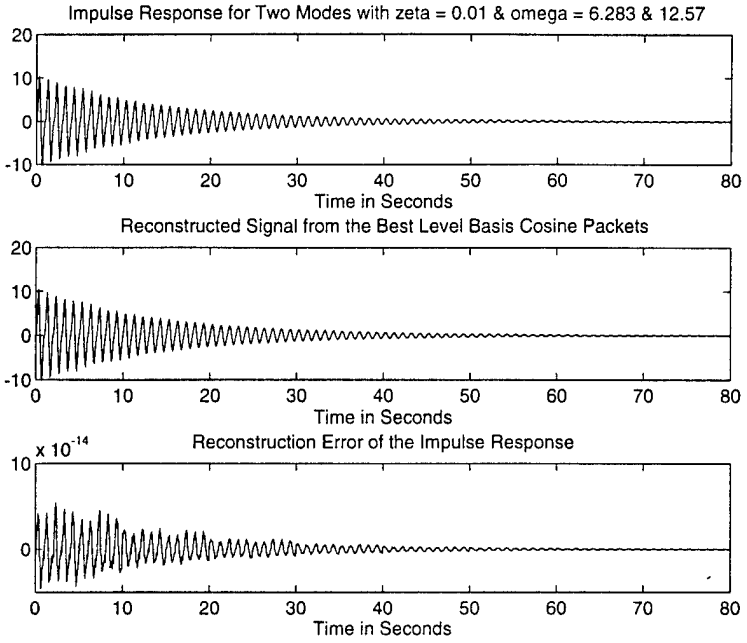

Figure 5.10: Reconstruction of the impulse response for a flexible structure with two modes

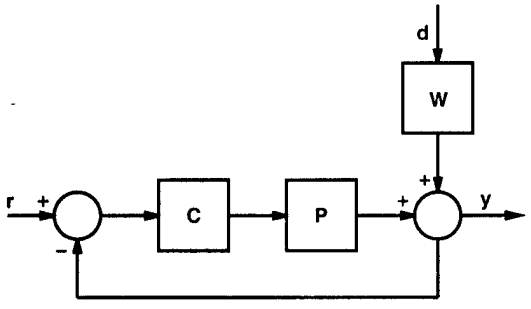

Figure 5.11: Feedback Control System

6. CONCLUSION

The main thrust of this project has been to consider the control of interconnected rigid and flexible structures. Due to the fact that we distributed our attention to different modeling, analysis and design techniques, we have obtained many new results in different areas.

Conclusions obtained from individual aspects of our report are listed below, as they correspond to the chapters in this report:

In **Chapter 2** several results for sliding mode control of sampled-data systems were outlined. Due to limited sampling frequency and the "hold" processes in the control channels, perfect sliding mode never occurs in a sampled-data system. The control law being piecewise constant, the states can only be kept in a boundary layer of the sliding surface instead of being constantly and exactly on that surface. In this chapter, a new method of implementing discrete time sliding mode control for sample-data systems was developed to reduce the thickness of the boundary layer, to alleviate the effect of uncertainties, and to remove the undesired chattering in sliding mode. Three classes of sampled-data systems with uncertainties were investigated; namely, linear, nonlinear, and stochastic systems. By proper consideration of the sampling phenomenon in the control design, one can maintain the states in the vicinity of the sliding surface with accuracy up to at least $O(T^2)$, $O(T^2)$, and $O(T^{\frac{1}{2}})$ respectively. We have demonstrated these results on an actual hardware structure.

In **Chapter 3**, we have introduced a new approach for vibration damping in flexible structures based on the sliding–mode control approach. Previous use of this approach has been for finite dimensional (approximate) models of flexible structures. Here, we retain the infinite-dimensional model for the structures and investigate exact solutions using sliding–mode control. In the particular strategy introduced here, the design is accomplished initially for a class of differential–difference systems. It is then demonstrated that the model of flexible structures with second order spatial partial derivatives, can be transformed into the above differential–difference form. A number of different cases have been analyzed. We then consider a class of flexible structures with fourth order spatial partial derivatives. An integral transform is introduced that changes the model into second order form. Thus, a two-stage design process can be utilized to eventually generate the sliding–mode controllers. Sliding mode algorithms considered make the closed loop system highly insensitive to external disturbances and parameter variations. Furthermore, from the applications viewpoint, the models considered are particularly appropriate for the utilization of distributed actuation and may be used in "smart structures" with piezoelectric materials. To avoid difficulties in solving for the transformation kernel and performing the integral transformation analytically, a neural network may be trained to perform these tasks. By using the

neural network, exact knowledge of the kernel of the transformation is not required. The neural network then becomes the first stage of the vibration suppression controller. The second stage of the composite controller is the sliding mode controller which has been designed for the differential-difference system.

In **Chapter 4**, we introduce a new general design procedure for radial basis function neural networks and wavelet neural networks. These type of neural networks are especially well-suited for solving general pragmatic learning problems in which the training data consists of irregularly positioned data points. A multiresolution learning network or wavelet network, has the added capacity of being able to generalize the nonlinear relationship between the given inputs and desired outputs, along with capturing the desired fine details of the nonlinear mapping. We present simulation results for these two types of networks based on predicting actuator nonlinearities occurring in a flexible structure. The neural networks were trained using a set of training data and were then tested using additional data not contained in the training set and excellent performance was achieved and demonstrated.

In **Chapter 5**, we explored a couple of uses for time-frequency wavelets. First, an overview of time-frequency wavelets was presented. We then presented the concept of modeling a structural system using a best basis made up of time-frequency wavelets. We developed a versatile structure model based on time-frequency wavelets as opposed to the traditional finite element/modal models. The decomposition and reconstruction schemes for time-frequency wavelets were presented. Then simulation results were presented for modeling the impulse response of a structural system using cosine packets. These simulation results demonstrated the cosine packet decomposition, the basis selection procedure, and the reconstruction process. The concept of a multiresolutional controller was formulated and discussed. A multiresolutional controller which minimizes the sensitivity function for a SISO flexible structure in the H^2 norm was derived. This controller utilizes the structural models which were developed using time-frequency wavelets. Implementation issues for the multiresolutional controller were also discussed.

REFERENCES

[1] V. I. Utkin, *Sliding modes and their application in variable structure systems.* Moscow: MIR, 1978.

[2] V. Utkin and K. Young, "Methods for constructing discontinuity planes in multidimensional variable structure systems," *Automation and Remote Control*, vol. 39, pp. 1466–1470, 1979.

[3] B. Drazenovic, "The invariance condition in variable structure systems," *Automatica*, vol. 5, pp. 287–295, 1969.

[4] S. V. Drakunov and V. I. Utkin, "Sliding modes in dynamic systems," *International Journal of Control*, vol. 55, no. 4, pp. 1029–1037, 1992.

[5] K. D. Young and Ü. Özgüner, "Frequency shaping compensator design for sliding mode," *Int. J. Control*, vol. 57, no. 5, pp. 1005–1019, 1993.

[6] C. Milosavljevic, "General conditions for the existence of a quasisliding mode on the swithing hyperplane in discrete variable," *Automat. Remote Contr.*, vol. 46, pp. 307–314, 1985.

[7] V. Utkin and S. Drakunov, "On discrete-time sliding modes," in *Preprints of IFAC Workshop on Nonlinear Control*, (Capri, Italy), 1989.

[8] S. Sarpturk, Y. Istefanopulos, and O. Kaynak, "On the stability of discrete-time sliding mode control systems," *IEEE Trans. Automat. Contr.*, vol. AC-32, no. 10, pp. 930–932, October 1987.

[9] U. Kotta, "Comments on the stability of discrete-time sliding mode controlsystems," *IEEE Trans. Automat. Contr.*, vol. AC-34, no. 9, pp. 1021–1022, 1989.

[10] K. Furuta, "Sliding mode control of a discrete system," *Systems and Control Letters*, vol. 14, pp. 145–152, 1990.

[11] H. Sira-Ramirez, "Nonlinear discrete variable structure systems in quasi-sliding mode," *Int. J. Control*, vol. 54, no. 5, pp. 1171–1187, 1991.

[12] O. Kaynak and A. Denker, "Discrete-time sliding mode control in the presence of system uncertainty," *Int. J. Control*, vol. 57, no. 5, 1993.

[13] G. Bartolini, A. Ferrara, and V. I. Utkin, "On robust adaptive control of mimo linear plants using discrete," in *Proceedings of the 12th IFAC World Congress Conference*, (Sidney, Australia), pp. 51–56, July 1993.

[14] W. C. Su, S. V. Drakunov, and Ü. Özgüner, "Sliding mode control in discrete time linear systems," in *Proceedings of the 12th IFAC World Congress*, (Sidney, Australia), July 1993.

[15] S. V. Drakunov, W. C. Su, and Ü. Özgüner, "Discrete-time sliding-modes in stochastic systems," in *Proceedings of the 1993 American Control Conference*, (San Francisco, CA), pp. 966–970, June 1993.

[16] W. C. Su, Ü. Özgüner, and S. V. Drakunov, "Discrete time sliding mode control in nonlinear sampled-data systems," in *Proceedings of the Thirty-First Annual Allerton Conference on Communication, Control, and Computing*, (Urbana, IL), October 1993.

[17] R. Morgan and Ü. Özgüner, "A decentralized variable structure control algorithm for robotic manipulators," *IEEE Trans. Robotics and Automation*, vol. RA-1, no. 1, pp. 57–65, March 1985.

[18] R. Bucy and P. Josef, *Filtering for stochastic processes with applications to guidance.* New York: Chelsea Pub Co, 1987.

[19] K. Redmill and Ü. Özgüner, "Experiment on a truss-panel structure," in *Proceedings of the 1992 American Control Conference*, (Chicago, IL), pp. 2530–2534, June 1992.

[20] W. C. Su, S. V. Drakunov, Ü. Özgüner, and K. Redmill, "$o(t^2)$ sliding mode contol on a flexible structure," in *Proceedings of the 1995 American Control Conference*, (Seattle, WA), pp. 1318–1322, June 1995.

[21] R. Bellman and K. Cooke, *Differential-Difference Equations.* New York: Academic Press, 1963.

[22] S. Yurkovich, Ü. Özgüner, and F. Al-Abbas, "Model reference sliding mode adaptive control for flexible structures," *Journal of the Astronautical Sciences*, vol. 36, pp. 285–310, Aug. 1986.

[23] D. Young and Ü. Özgüner, "Frequency-shaped variable structure control," in *Proceedings of the American Control Conference*, (San Diego, CA), May 1990.

[24] S. V. Drakunov and V. I. Utkin, "Sliding mode control concept for abstract dynamic systems," in *Proceedings of the International Workshop on Nonsmooth Control and Optimization*, (Vladivostok, Russia), September 1991.

[25] S. V. Drakunov, D. B. Izosimov, A. G. Luk'yanov, V. A. Utkin, and V. I. Utkin, "The block control principle: Part I," *Automation and Remote Control*, vol. 51, no. 5, pp. 601–608, 1990.

[26] S. V. Drakunov, D. B. Izosimov, A. G. Luk'yanov, V. A. Utkin, and V. I. Utkin, "The block control principle: Part II," *Automation and Remote Control*, vol. 51, no. 6, pp. 737–746, 1990.

[27] L. Meirovitch, *Elements of Vibration Analysis.* New York: McGraw-Hill, 1986.

[28] S. V. Drakunov and Ü. Özgüner, "General sliding modes for manifold control of distributed parameter systems," in *Variable Structure and Lyapunov Control* (A. S. I. Zinober, ed.), ch. 11, pp. 219–241, Berlin: Springer-Verlag, 1993.

[29] J. Hertz, A. Krogh, and R. G. Palmer, *Introduction to the Theory of Neural Computation.* Redwood City, California: Addison-Wesley, 1991.

[30] B. J. A. Kröse and P. P. van der Smagt, *An Introduction to Neural Networks.* Department of Computer Systems, University of Amsterdam, Amsterdam, The Netherlands, September 1991.

[31] S. V. Drakunov, Ü. Özgüner, and L. Lenning, "Use of neural networks and sliding modes in vibration damping," in *Smart Structures and Materials 1993: Mathematics in Smart Structures* (H. T. Banks, ed.), pp. 174–181, Proc. SPIE 1919, 1993.

[32] D. S. Broomhead and D. Lowe, "Multivariable functional interpolation and adaptive networks," *Complex Systems*, vol. 2, pp. 321–355, 1988.

[33] S. P. Lloyd, "Least squares quantization in pcm," *IEEE Transactions on Information Theory*, vol. 28, pp. 281–294, February 1982.

[34] J. MacQueen, "Some methods for classification and analysis of multivariate observations," in *Proceedings of the Fifth Berkeley Symposium on Mathematical Statistics and Probability*, University of California, Berkeley, June-July 1965.

[35] J. Moody and C. J. Darken, "Fast learning in networks of locally-tuned processing units," *Neural Computation*, vol. 1, pp. 281–294, 1989.

[36] S. Chen, C. F. Cowan, and P. M. Grant, "Orthogonal least squares learning algorithm for radial basis function networks," *IEEE Transactions on Neural Networks*, vol. 2, pp. 281–294, March 1991.

[37] I. Daubechies, *Ten Lectures on Wavelets.* Philadelphia, PA: Society for Industrial and Applied Mathematics, 1992.

[38] Q. Zhang and A. Benveniste, "Wavelet networks," *IEEE Transactions on Neural Networks*, vol. 3, pp. 889–898, November 1992.

[39] Q. Zhang, "Wavelet networks: The radial structure and an efficient initialization procedure," Tech. Rep. LiTH-ISY-I-1423, Linköping University, October 1992.

[40] S. G. Mallet, "A theory for multiresolution signal decomposition: The wavelet representation," *IEEE Transactions on Pattern Analysis and Machine Intelligence*, vol. 11, pp. 674–693, July 1989.

[41] I. Daubechies, "The wavelet transform, time-frequency localization and signal analysis," *IEEE Transactions on Information Theory*, vol. 36, pp. 961–1005, September 1990.

[42] J. Kovacevic and M. Vetterli, "Nonseparable multidimensional perfect reconstruction filter banks and wavelet bases for R^N," *IEEE Transactions on Information Theory*, vol. 38, pp. 533–555, March 1992.

[43] B. Bakshi and G. Stephanopoulos, "Wave-net: a multiresolution, hierarchical neural network with localized learning," *AIChE Journal*, vol. 39, pp. 57–81, January 1993.

[44] Q. Zhang, "Regressor selection and wavelet network construction," in *Proceedings of the 32nd Conference on Decision and Control*, IEEE, December 1993.

[45] J. Park and I. W. Sandberg, "Universal approximation using radial-basis-function networks," *Neural Computation*, vol. 3, pp. 246–257, 1991.

[46] D. Clancy and Ü. Özgüner, "A multiresolutional controller design approach using wavelets," in *Proceedings of the 1995 International Symposium on Intelligent Control, to appear*, IEEE, August 1995.

[47] Y. Meyer, *Wavelets: Algorithms and Applications.* Philadelphia, PA: Society for Industrial and Applied Mathematics, 1993.

[48] M. Wickerhauser, *Adapted Wavelet Analysis From Theory to Software.* Wellesley, MA: A. K. Peters, Ltd, 1994.

[49] G. Strang and T. Nguyen in *Workshop on Wavelets and Filter Banks*, (Wellesley, MA), San Jose State University, Wellesley-Cambridge Press, January 1995.

[50] G. Strang, "Wavelets and dilation equations: A brief introduction," *SIAM Review*, vol. 31, pp. 614–627, December 1989.

[51] D. Gabor, "Theory of Communication," *IEE*, vol. 93, pp. 429–457, 1946.

[52] R. Coifman and Y. Meyer, "Remarques sur l'analyse de Fourier à fenêtre," *C. R. Acad.*, vol. 312, no. Ser. A I, pp. 259–261, 1991.

[53] H. S. Malvar, "Lapped Transforms for Efficient Transform/Subband Coding," *IEEE Transactions Acoustics, Speech and Signal Processing*, vol. 38, pp. 969–978, 1990.

[54] H. S. Malvar and D. H. Staelin, "The LOT: Transform Coding Without Blocking Effects," *IEEE Transactions Acoustics, Speech and Signal Processing*, vol. 37, pp. 553–559, 1989.

[55] P. Auscher, G. Weiss, and M. V. Wickerhauser, "Local Sine and Cosine Bases of Coifman and Meyer and the Construction of Smooth Wavelets," in *Wavelets-A Tutorial in Theory and Applications* (C. K. Chui, ed.), pp. 237–256, Cambridge, MA: Academic Press, 1992.

[56] O. Zienkiewicz, *The FEM in Engineering Science*. New York, NY: McGraw-Hill, 1971.

[57] G. Strang and G. Fix, *An Analysis of the FEM*. Englewood Cliffs, NJ: Prentice-Hall, 1973.

[58] M. Balas, "Trends in Large Space Structure Control Theory: Fondest Hopes, Wildest Dreams," *IEEE Transactions on Automatic Control*, vol. AC27, pp. 522–535, June 1982.

[59] R. J. Benhabib, R. P. Iwens, and R. L. Jackson, "Stability of large space structure control systems using positivity concepts," *AIAA Journal of Guidance and Control*, vol. 4, pp. 487–494, September-October 1981.

[60] R. R. Coifman and M. V. Wickerhauser, "Entropy Based Algorithms for Best Basis Selection," *IEEE Transactions on Information Theory*, vol. 38, no. 2, pp. 713–718, 1992.

[61] J. C. Doyle, K. Glover, P. P. Khargonekar, and B. A. Francis, "State-Space Solutions to Standard H^2 and H^∞ Control Problems," *IEEE Transactions on Automatic Control*, vol. AC34, pp. 831–847, August 1989.

[62] B. Francis, "On the Wiener-Hopf Approach to Optimal Feedback Design," *Systems and Control Letters*, vol. 2, pp. 197–201, December 1982.

[63] H. Özbay and A. Tannenbaum, "On the Structure of Suboptimal H^∞ Controllers in the Sensitivity Minimization Problem for Distributed Stable Plants," *Automatica*, vol. 27, no. 2, pp. 293–305, 1991.

[64] D. C. Youla, J. J. Bongiorno, Jr., and H. A. Jabr, "Wiener-Hopf Design of Optimal Controllers - Part I: The Single-Input-Output Case," *IEEE Transactions Automatic Control*, vol. 21, pp. 3–13, 1976.

Ümit Özgüner

Chapters in Books

1. "Generalized Sliding Modes for Manifold Control of Distributed Parameter Systems," in *Variable Structure and Lyapunov Control*, A.S. Zinober ed., Ch.11, 219–241, Springer Verlag 1993. (S. Drakunov and Ü. Özgüner).

Journal Publications

1. "Neural Control of Flexible Systems with Partially Known Dynamics," *Modelling and Scientific Computing, Special Issue on: Neural Networks for Identification and Control of Dynamical Systems*, Vol.1, No.3-4,263-280, 1994, (J. Donne, J–X. Xu and Ü. Özgüner).

2. "Robust Stabilization of Nonlinear Systems with Parametric Uncertainty," *IEEE Transactions AC*, V39,No.8, August 1994, (D. Schoenwald and Ü. Özgüner).

3. "Flexible Manipulator Control Using Integral Manifolds and Distributed Vibration Damping," in print, to appear Jan. 1996 *Dynamics and Control*, (D. Schoenwald and Ü. Özgüner).

4. "Constructing Discontinuity Surfaces for Variable Structure Systems, A Lyapunov Approach," in print, to appear *Automatica* 1996, (W-C. Su, S. Drakunov and Ü. Özgüner).

Conference Publications

1. "Optimization of Nonlinear System Output via Sliding–Mode Approach," IEEE Workshop on *Variable Structure and Lyapunov Control of Uncertain Dynamical Systems*, September 1992, University of Sheffield, UK, (S. Drakunov and Ü. Özgüner)

2. "Vibration Suppression in Flexible Structures via the Sliding–Mode Control Approach," IEEE Workshop on *Variable Structure and Lyapunov Control of Uncertain Dynamical Systems*, September 1992, University of Sheffield, UK, (S. Drakunov and Ü. Özgüner)

3. "Decentralized Sliding–Mode Observers for Interconnected Nonlinear Systems," IEEE Workshop on *Variable Structure and Lyapunov Control of Uncertain Dynamical Systems,* September 1992, University of Sheffield, UK, (S. Drakunov, Ü. Özgüner and D. Schoenwald)

4. "Experiments on a Truss–Panel Structure," Proc. 1992 ACC, Chicago IL, June 1992. (Ü. Özgüner and K. Redmill).

5. "A Decentralized Approach for Autonomous Structural Control," *Autonomous Structural Control Symposium*, August 1992, USAF Academy, Colorado.

6. "Variable Structure Control in Sampled Systems," *NSF/OAI Workshop on Variable Structure Control*, October 1992, Brook Park, OH.

7. "Vibration Suppression in Flexible Structures via the Sliding–Mode Control Approach," Proc 1992 CDC, Tucson Arizona, (S. Drakunov and Ü. Özgüner).

8. "Distributed Hierarchical Architecture for Structural Control," Proc. North American Conf. on *Smart Structures and Materials*, 1–4 Feb. 1993, Albuquerque, New Mexico.

9. "Use of Neural Networks and Sliding Modes in Vibration Damping," Proc. North American Conf. on *Smart Structures and Materials*, 1–4 Feb. 1993, Albuquerque, New Mexico, (S. Drakunov, Ü. Özgüner and L. Lenning).

10. "Discrete–Time Sliding Modes in Stochastic Systems," Proc. 1993 ACC, San Francisco, June 1993. (S. V. Drakunov, W.-C. Su and Ü. Özgüner).

11. "Decentralized Control of Uncertain Systems via Sensitivity Models," Preprints 12th World Congress IFAC, Sydney Australia, 1993. (D. A. Schoenwald and Ü. Özgüner).

12. "Sliding Mode Control in Discrete Time Linear Systems," Preprints 12th World Congress IFAC, Sydney, Australia, 1993. (W-C. Su, S. Drakunov and Ü. Özgüner).

13. "Sliding Mode with Chattering Reduction in Sampled Data Systems," Proc. 1993 CDC, San Antonio, Texas, (W-C. Su, S. Drakunov, Ü. Özgüner and D. Young).

14. "Wavelet Neural Networks: A Design Perspective," Proc. 9th IEEE International Symposium on Intelligent Control, Aug. 1994, Columbus, OH, (D. Clancy and Ü. Özgüner).

15. "Design and Evaluation of RBF and Neural Network Methodologies for Feathering the Solar Arrays of the Space Station," Proc. IFAC Conference on Aerospace Control, Sept. 1994, San Francisco, CA (D. Clancy and Ü. Özgüner).

16. "Implementation of Varable Structure Control for Sampled Data Systems," Proc. VSS and Lyapunov Techniques Workshop, Sept. 1994, Benevento, Italy. (W.C.Su, S. Drakunov and Ü. Özgüner).

17. "Flexible Beam Modelling with Analog VLSI circuits," INT Mechanical Engr. Congress and Expo., Nov. 1994, Chicago, Ill, (A. Shah, L. Lenning, S. Bibyk and Ü. Özgüner).

18. "Analog VLSI Circuit Models for Smart Flexible Structures," SPIE Conf. on Active Materials and Adaptive Structures, Feb. 1995, San Diego CA (A. Shah, L. Lenning, S. Bibyk and Ü. Özgüner).

19. "O(T^2) sliding in Sampled Systems with Applications," 1995 ACC, Seattle, Washington, June 1995, (W.C. Su, S. Drakunov and Ü. Özguner).

20. "A Multiresolutional Controller for Sensitivity Minimization of Flexible Structures," Proc. 1995 ISIC, Monterey, CA. (D. Clancy and Ü. "Ozgüner).

(AFSC)

lowed and is
AFR 190-12

Approved for public release,
distribution unlimited

Joan
STINFO Program Manager